processes

MDPI

Article

Tensile Behavior of Parts Manufactured Using a Material Extrusion Process from a Filament with Short Carbon Fibers and PET Matrix

Madalina-Ioana Blaj [1], Sebastian-Marian Zaharia [1], Cristin Olimpiu Morariu [1], Mihai Alin Pop [2], Mihaela Cosnita [3] and Gheorghe Oancea [1,*]

[1] Department of Manufacturing Engineering, Transilvania University of Brasov, 500036 Brasov, Romania; madalina.blaj@unitbv.ro (M.-I.B.); zaharia_sebastian@unitbv.ro (S.-M.Z.); c.morariu@unitbv.ro (C.O.M.)
[2] Department of Materials Science, Transilvania University of Brasov, 500036 Brasov, Romania; mihai.pop@unitbv.ro
[3] Department of Product Design, Mechatronics and Environment, Transilvania University of Brasov, 500036 Brasov, Romania; mihaela.cosnita@unitbv.ro
* Correspondence: gh.oancea@unitbv.ro

Abstract: One of the latest tendencies in research related to material extrusion based on additive manufacturing is to determine the mechanical characteristics of parts taking into consideration the most influential manufacturing parameters. The main research objective is to describe how the manufacturing parameters, part orientation, layer thickness and infill density influence the tensile behavior of specimens made from PET with 15% short carbon fibers. The most advantageous result is obtained for a layer thickness of 0.15 mm, with 100% material infill, and material deposition on the longitudinal direction of the part. The obtained mean values are: 65.4 MPa tensile strength, 1.93% strain at rupture, and 9 GPa Young Modulus. For these values, the tensile behavior of specimens manufactured along transverse and thickness directions are presented. The least favorable results are obtained for manufacturing by thickness. The novelty of the discussed research consists in all these aspects together with an original mathematical model that was determined based on design of experiments with a correlation of the regression model of over 90%. By optical and electronic microscopy material gaps are visible in the filament and manufactured parts, and the failure occurs in most cases in form of matrix cracks and delamination.

Keywords: MEX process; PET; short carbon fibers; mechanical properties; microscopy; manufacturing defects

Citation: Blaj, M.-I.; Zaharia, S.-M.; Morariu, C.O.; Pop, M.A.; Cosnita, M.; Oancea, G. Tensile Behavior of Parts Manufactured Using a Material Extrusion Process from a Filament with Short Carbon Fibers and PET Matrix. *Processes* **2024**, *12*, 334. https://doi.org/10.3390/pr12020334

Academic Editor: Li Xi

Received: 27 December 2023
Revised: 27 January 2024
Accepted: 1 February 2024
Published: 3 February 2024

1. Introduction

At present, Additive Manufacturing (AM) is one of the most important topics in the industry with various applications, from the automotive and aerospace industries to medicine and food industry. From all processes of AM, Material Extrusion (MEX) occurs in 69% of its applications due to its advantages regarding the variety of materials which can be used for parts manufacturing, the cost-to-quality ratio of the part, the complexity of parts that can be manufactured through this process and their final mechanical and chemical properties [1,2]. MEX is the manufacturing process which uses heated material in filament form that is stacked layer by layer according to a specific desired geometry [3]. Even though the printing process is preferred due to its simplicity, variations of the mechanical characteristics of the obtained parts occur due to it's the values of the manufacturing parameters. The main parameters are: layer thickness, infill, raster angle, part orientation on the manufacturing platform, temperature (at the nozzle, on the printing platform and in the environment) and work environment [1–4]. A further research challenge is also identifying the optimum combination of these parameter setpoints in order to maximize the mechanical characteristics [4,5].

The filaments used for manufacturing vary from simple thermoplastic materials to thermoplastic materials combined with particles and fibers (short or continuous), called composite filaments. In literature [4,5] also the similarity with conventional composite materials is presented, and theoretical models for tensile strength prediction are developed considering the transverse isotropy hypothesis, classical lamination theory and the Hill-Tsai anisotropic plasticity criterion or the hypothesis of orthotropic materials in plane stress state. Also, from the description of the mechanical properties, the anisotropy of the specimens is highlighted. Other novelties are related to printable materials with shape memory, based on the effect of thermal programming, which are translated into shape recovery and fixity and stress recovery [6].

This study aims to present the behavior of short carbon fibers used as a reinforcement material in a polymer matrix, which have a significant impact on the MEX process when it is. The importance of Short Carbon Fibers (short-CF) in Additive Manufacturing resides in the improvement of the mechanical properties of the manufactured parts and their addition to the matrix which offer higher stiffness, strength, and thermal resilience [1,5,7,8]. As an example, in the research reported in [9] led to obtaining a tensile strength for composite filaments increased by 57%, compared to filaments of pure Poly(Acrylonitrile-co-Butadiene-co-Styrene) (ABS). In [10] the researchers obtained an increased Young Modulus of 8% for an addition of 5% glass fibers into Polylactic Acid filaments. In [11] the researchers obtained an increased tensile strength of 20% for an addition of 10% fibers into the same type of samples as in [10]. Furthermore, Young's Modulus is increased by 28%. In [12], the addition of 10% carbon fibers into the Onyx matrix increased the tensile strength from 28.92 MPa to 418 MPa.

Besides its advantages, the addition of fibers has also a negative effect on the geometrical accuracy [1]. Another study [2] reports a behavior consequently to using short-CF in the matrix; however, anisotropy of the studied materials was observed due to the alignment of the majority of fibers by the direction of printing. In [13] a comparative study is presented involving specimens made from polyamide with carbon fibers through by MEX and by injection-molding, respectively. The worst results are obtained for printed specimens due to their higher porosity of 9 to 12%, these display lower values for yield stress and 17 to 22% lower values for Young's Modulus compared to specimens obtained by injection molding.

Related to layer thickness as a manufacturing parameter in [14] it is asserted that the geometrical stability is affected most by this criterion. Thus, as the value of the layer thickness is increased, the cross section of the deposited material is more rounded, which translates into a smaller contact surface between deposited material layers. Deposited material cross-sections are related to the "stair-effect" presented in [4,5], affecting also the surface quality and mechanical properties. Thus, by decreasing the layer thickness, the mechanical properties are improved due to the reducing of the gaps in the deposited material [5]. In another study [15], researchers identified that yield stress, tensile and flexural strength increased 1.16, 1.27 and 1.28 times, respectively, for a layer thickness of 0.2 mm compared to a layer thickness of 0.3 mm of Poly(vinyl chloride) (PVC).

Regarding the infill type, according to [4,5] the material can be deposited in different patterns: linear, rectangular, honeycomb, zig-zag at a certain density. A higher infill density entails increased part manufacturing time and material; due to their greater stiffness these parts can carry more load.

Other papers [4,7] mentioned that the tensile strength is maximized if the direction of load follows the printing direction. In [5] the authors investigated the impact of several manufacturing parameters on the tensile behavior, the most influential being: the part orientation on the printing platform, layer thickness and infill. In [7] the investigation is concerns tensile testing of short carbon fiber polyamide parts, the most influential manufacturing parameters being layer thickness and raster angle, which confirms the information in [4]. The research presented in [8] provides a review of MEX, confirming the previously presented results. Paper [16] discusses tensile testing of specimens with 100% infill while varying layer thickness for the same material. The best result of 58 MPa is

obtained for the specimens with the thinnest layer of 0.15 mm. The study is performed on BCN3D Sigma, which is a printer without enclosure.

The research reported in [17] carries out comparisons of ABS versus ABS CF, PLA versus PLA CF, Polyethylene terephthalate glycol (PETG) versus PETG CF and Amphora versus Amphora CF, respectively, also considering part orientation from 0° to 90°. In this case, the most advantageous results are obtained in specimens manufactured at a direction of 0°, while the worst results correspond to a direction of 90 ° Carbon fiber addition to the matrix brought an improvement of tensile strength for 0° orientation, ranging from 5.1% in Amphora CF to a maximum of 48% in PETG CF for the specimens made from the matrix material. The tensile strength for PETG CF is 68.3 MPa, Young's Modulus is 8.47 GPa and strain at rupture is 2.99%. These results are presented for longitudinal material deposition.

In order to obtain a larger spectrum of results of the proposed study, Table 1 below presents a summary of short carbon fiber utilization in composite filaments. It can be concluded that the used matrix has an increased impact on the mechanical properties, the most used matrix in studies being Poly(lactic Acid) (PLA). Based on this table material defects can be highlighted: weak bonding between layers and material gaps, also revealed as the most important defects by the research presented in [15]. In [18], upon identifying these issues, the authors established that a higher enclosure temperature increases the tensile strength of parts due to improved bond formation. These findings are verified by scanning electron microscopy (SEM) that revealed a porosity reduced to 4.2%. Also, from the studies mentioned in Table 1, the most common manufacturing parameters are thickness layer and infill density.

Table 1. Composite filaments with short carbon fibers studies-summary.

Ref.	Material	Testing Methods	Remarks
[19]	PLA-CF 30%	SEM Tensile	Fiber conglomerate & Weak bonding fiber–matrix/Rm = 49.41 MPa, E = 1.26 GPa, ε at rupture = 7.81%
[20]	PLA CF	DOE Tensile	Parameters: printing speed (60,80, 100 mm/min), infill (40%, 60%, 80%), layer thickness (0.1 mm, 0.2 mm, 0.3 mm) ⇒ Rp = 26.49 MPa at 100 mm/min, Infill 60% & layer thickness = 0.2 mm.
[21]	ABS/PLA/PC/PETG-CF15% PA-CF25%	Notch in tension Notch in compression	Matrix type has an important impact over mechanical properties–ABS; PLA & PETG–most consistent results
[22]	PLA-CF10% PLA-CF20% PLA-CF30%	Tensile Porosity Roughness	Most advantageous results–PLA-CF10%: Rm ≈ 23 MPa, E ≈ 1.8 GPa Weak matrix bonding with fibers ⇒ mechanical properties are decreasing as the % of CF is increasing
[23]	PLA-CF	Tensile	Infill–highest impact over mechanical properties–Rm = 61.83 MPa with 90% infill density and 0.05 mm layer thickness Highest strength for 100% infill density.
[24]	PLA-CF 10%/ABS-CF 32%	Tensile SEM	From studied materials–most advantageous results for PLA-CF. More materials gaps for specimens with fibers compared to the simple specimens made from matrix.

In the research presented in this paper the considered polymer is Polyethylene Terephthalate, also known as PET, which forms the matrix of the composite filament of PET CF15, namely a matrix with 15% of short and chopped carbon fibers in its composition. Based on the findings reported in paper [25] the 15% fiber content was selected due to the most favorable results that were obtained for this composition, namely 98 MPa tensile strength and 14.4 GPa Young's Modulus, the research included tensile tests for specimens with 5%, 10% and 15% short carbon fibers in polypropylene (PP) matrix.

Other studies related to PET CF composite filaments, such as discussed in [26], assert that a reinforcement with short carbon fibers up to 40.7% determined an increased Young Modulus of up to 390%, but also a weak interface between the fibers and the matrix.

The purpose of this research is to determine the most advantageous behavior regarding tensile strength for PET CF15 specimens, considering several of the most influential manu-

facturing parameters, such as layer thickness, part orientation and infill. Also taken into account are the results obtained by other researchers, namely that mechanical properties improve as the layer thickness decreases and the infill density tends towards 100%.

For a thorough study of the influence of manufacturing parameters on the tensile strength of PET CF15 specimens, investigations included also various methods of experiment design. The test specimens were manufactured from material deposited by the longitudinal direction, taking into consideration the best results obtained by other researchers for this direction. For corroboration purposes a visual inspection is also performed in order to determine manufacturing defects and failure causes in search for other defects besides material gaps, as done in the work of other researchers. A comparison of results by the type of 3D printer can also be performed, based on the results presented in [16].

2. Materials and Methods

The material used in the research discussed in this paper is PET CF15 produced by Ultrafuse BASF (BASF, Ludwigshafen am Rhein, Germany), whose filament has a nominal diameter of 2.85 mm. The material is recommended especially for industrial applications. While it is resistant to up to 100 °C, maximized characteristics can be obtained if the material is kept under proper conditions, such as a dry environment. The producer offers a description of the mechanical properties, as shown in Table 2 below.

Table 2. Material description: PET CF15 [27].

Property	XY Plane	XZ Plane	ZX Plane
Tensile Strength	63.2 MPa	-	12.5 MPa
Strain at Break	3.7%	-	0.5%
Young Modulus	6178 MPa	-	2822 MPa

The digital model of the specimen reproduces the dimensions of the Type I specimen included in ASTM D634-14 standard [28], because the material investigated in the research falls into the category of reinforced composites. This standard is used due to the similarity of additive manufactured parts and composite materials. The nominal thickness of the specimen is 3.2 mm, with a total length of 165 mm. The gage length is 57 mm and its width is 13 mm.

The machine used for manufacturing in this research is BCN3D Epsilon [29]. It has an enclosure and functions based on the MEX method. It covers a volume of 420 mm × 300 mm × 400 mm, with filaments of 2.85 mm diameter. The manufacturing parameters used in the research are defined in the printer's software for slicing, BCN3D Cura 1.5.5, (BCN3D Technologies, Barcelona, Spain) and are presented in Table 3 above.

Table 3. Manufacturing parameters for specimens defined in BCN3D Cura software.

Parameter	Value
Layer Thickness [mm]	0.15/0.2/0.25
Wall Thickness [mm]	1.8
Top Thickness [mm]	0.8
Bottom Thickness [mm]	0.8
Top/ Bottom Pattern	Lines
Infill Pattern	Lines
Infill density %	100/75/25
Nozzle Temperature [°C]	265
Build Plate Temperature [°C]	60
Print Cooling	Off
Nozzle diameter	0.6 mm

Figure 1a presents a set of 5 specimens prepared for manufacturing, represented in the slicing software. The orientation of the parts is 45° in order to have raster angles

of 0° and 90°, respectively, and to have the material deposited in the tensile direction. Figure 1b presents a set of manufactured specimens on the printer platform. The applied method included the manufacturing of a set of five specimens, for each combination of selected manufacturing parameters. Five specimens is the minimum number required by the standard for obtaining conclusive results.

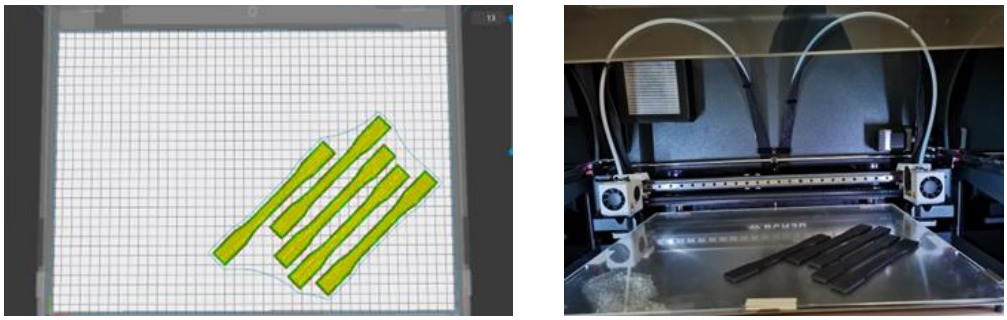

(**a**) (**b**)

Figure 1. Tensile specimens: (**a**) Preview of five specimens in BCN3D Cura software; (**b**) five specimens after manufacturing.

The tests carried out as part of this research take into consideration two variables: layer thickness and infill. For each manufacturing parameter three values are relevant:

- Thickness layer: 0.15 mm, 0.20 mm and 0.25 mm;
- Infill density: 100%. 75%, and 25%.

The tensile tests are conducted for each combination of parameters, using the following codification: C_t_I_no, where "t" is the value for layer thickness, "I" is the infill percentage and "no" is the specimen number from the considered set.

While the studied material is anisotropic, for the purposes of this research it is considered orthotropic with its maximum tensile strength obtained along the direction of machining. The study is performed considering the material being deposited along the longitudinal direction (X) of the specimen, obtaining the tensile values along direction XX or 11. A local coordinate system is considered for each specimen, with the X axis along specimens length. According to [30] for laminate composite materials the tensile values are equivalent for directions X or 11 and for directions Y or 22, respectively—see Figure 2 [30]. In this case, the results obtained for the specimens with longitudinally deposited material, are considered with regard to the manufacturing parameters to be drivers for the next steps of the research. The testing of the specimens and the results are presented separately for each group, according to the orientation of the material deposition process.

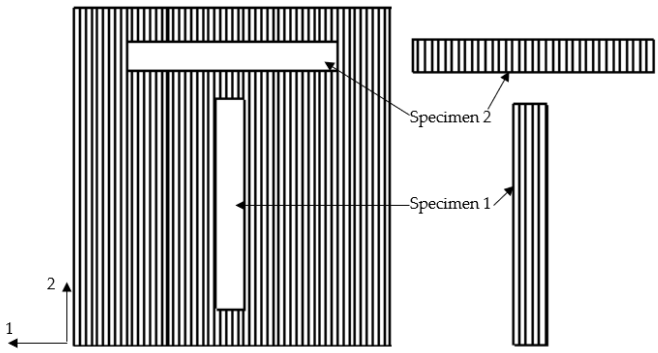

Figure 2. Composite specimen extraction from a composite panel [30].

The values of tensile strength on the transverse and thickness directions are necessary for a complete material description. In order to obtain the best tensile strength, the optimum combination of manufacturing parameter setpoints has to be identified. For this a set of

five specimens was manufactured by the transverse and thickness directions in order to be tested, as presented in Figure 3 below. Due to the reduced contact area of the specimen with the printer plate and the increased risk of printing failure, auxiliary supports are generated for the part during manufacturing. These supports are removed after the manufacturing of the specimen.

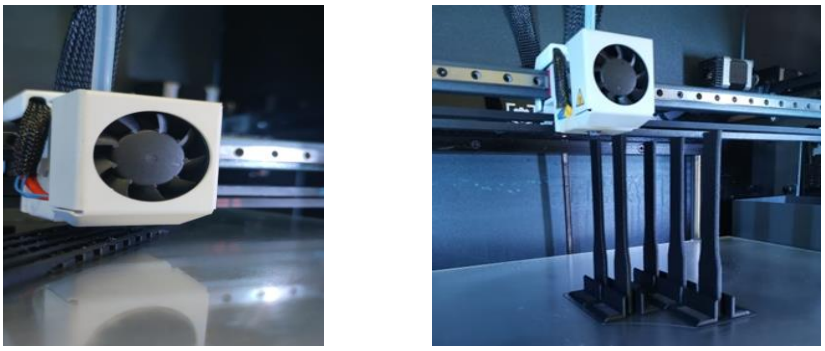

(**a**) (**b**)

Figure 3. Tensile specimens: (**a**) In the transverse direction with supports; (**b**) In the thickness direction with supports.

The generated specimens were tested for tensile strength on the Universal Testing Machine WDW-150S (Jinan Testing Equipment IE Corporation, Jinan, China) equipped with a hydraulic parallel grip. The specimens are placed between the grips of the testing machine, the longitudinal axis of the specimen being aligned with an imaginary axis between grips. The grips are tightened to prevent the slippage of specimens from the machine. By means of the MaxTest V1 machine software data is collected for plotting the stress-strain curve for each specimen. This is then post-processed according to [28], due to machine artifacts.

The post-processed results are presented in Section 3. Manufacturing defects are verified visually as well as by means of the Nikon T1-SM microscope (Nikon, Tokyo, Japan) and the Emspira 3 microscope (Leica Microsystems GmbH, Wetzlar, Germany). SEM analysis is performed using a Hitachi S3400N type II machine, produced in Japan, Tokyo. After tensile testing, failure can also be identified by visual inspection. Dimensional deviations of the specimen width and thickness were checked against the nominal dimensions. Design of experiments (DoE) was conducted in Minitab 21 (Minitab, LLC, State College, PA, USA). The input data used in DoE were the results obtained after post-processing the specimens manufactured by longitudinal material deposition. DoE is performed as an iterative process, starting with a linear regression model, then moving to a polynomial model, and to a second-order polynomial regression. A higher order regression is not recommended as it would yield a complex and difficult to use model. The regression model is selected based on the level of correlation, which is recommended to be over 90%, and on the significance of the constituent terms expressed by their respective p-value. A term is significant if its p-value is below 0.05.

3. Results and Discussions

3.1. Tensile Testing and Results

3.1.1. The Longitudinal Direction

Each specimen is tested according to [20] and presented in Figure 4 and in Appendix A in Figures A1–A8, before and after testing. The behavior of specimens for 100% Infill is almost similar. The rupture of all specimens occurred in almost the same place, showing that specimens are compact and homogenous if the infill is 100%. The thickness layer has a reduced impact on the location of the rupture. As the infill density is reduced, rupture occurs in a random location, the highest impact being on specimens with 25% infill density.

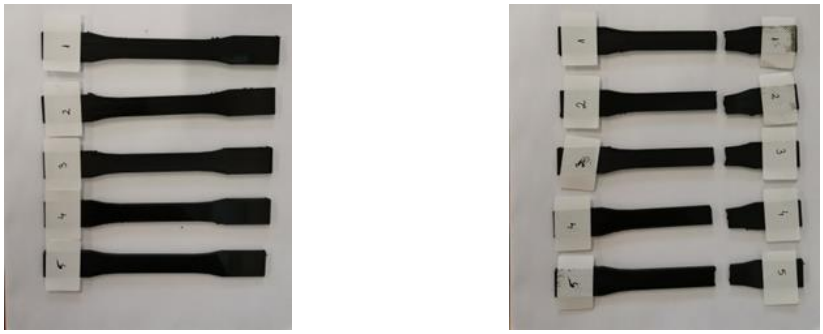

(**a**) (**b**)

Figure 4. Longitudinal Tensile Specimens C_15_100: (**a**) Before testing; (**b**) After testing.

Figure 5, Tables 4 and 5, and Appendix B present the stress-strain curves for each set of specimens and the results for each specimen: Fm (kN)—force at rupture, Rm (MPa)—tensile strength, Fp (kN)—force at yield point, Rp (MPa)—Yield stress, E (GPa)—Young's Modulus and ε (%)—total strain percent at rupture of the considered specimen. All the values are calculated by the testing machine software.

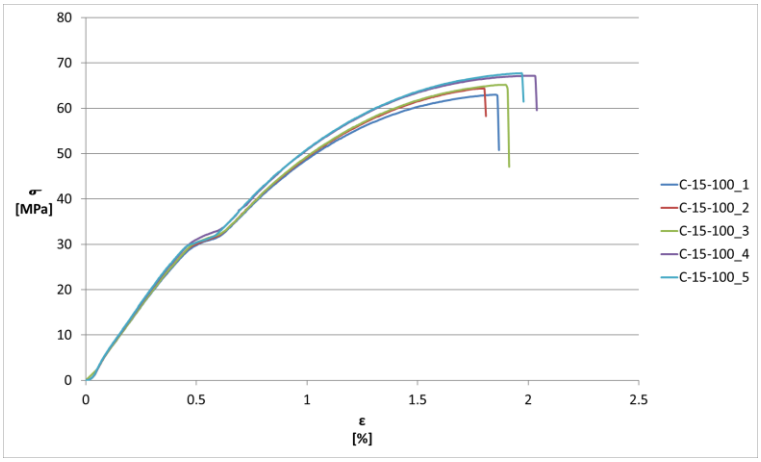

Figure 5. Longitudinal Tensile Specimens results—Stress-Strain curves for C_15_100.

Table 4. Longitudinal Tensile Specimens Result—C_15_100.

Specimen	Fm [kN]	Rm [MPa]	Fp [kN]	Rp [kN]	E [GPa]	ε [%]
C_15_100_1	2.661	63	2.066	49	9	1.88
C_15_100_2	2.718	64	2.133	50	9	1.82
C_15_100_3	2.753	65	2.146	51	9	1.91
C_15_100_4	2.837	67	2.228	53	9	2.05
C_15_100_5	2.86	68	2.326	55	9	1.99
Average	2.77	65.40	2.18	51.60	9	1.93

Table 5. Longitudinal Tensile Specimens Result—C_15_100—Deviations from the mean value.

Specimen	Fm [%]	Rm [%]	Fp [%]	Rp [%]	E [%]	ε [%]
C_15_100_1	−3.79	−3.67	−5.22	−5.04	0.00	−2.59
C_15_100_2	−1.73	−2.14	−2.15	−3.10	0.00	−5.70
C_15_100_3	−0.46	−0.61	−1.55	−1.16	0.00	−1.04
C_15_100_4	2.57	2.45	2.21	2.71	0.00	6.22
C_15_100_5	3.41	3.98	6.71	6.59	0.00	3.11

An average value is calculated for each set, as well as the deviation for each such value. These are presented in Appendix B. Material behavior is described by the stress-strain curves. In the linear area Hooke's Law is applicable and the material is elastic. The specimen will regain its initial dimensions and shape after removal of the load. Beyond the elastic region the strains increase faster up to the yielding point. Beyond this point the material enters the plastic area with a greater resistance to deformation.

The best results are obtained for the set of specimens with 100% material infill and a thickness layer of 0.15 mm. These have the following average values: Rm = 65.4 MPa, Rp = 51.6 MPa, E = 9 GPa and ε = 1.93%. These values are used for further testing specimens machined transversally and in-depth.

For this set the obtained strength ranged from 68 MPa to 63 MPa. Young's Modulus had a constant value for the entire set. The strain at rupture ranged from 1.82% to 2.05%. The maximum strain values were not recorded on the specimens with maximum strength.

Comparing the results for all sets of specimens by infill reveals the increased impact of the thickness layer: the values have a tendency of decreasing if the infill percentage is lower and the thickness layer increases, as already stated in Introduction.

The least beneficial results are recorded for the set of specimens with a material infill density of 25% and the layer thickness of 0.25 mm, where the average value of strength is 36.3 MPa, yield strength is 29 MPa, Young's Modulus is 7 GPa and the strain at rupture is 1.44%.

According to the stress-strain curves for each set the behavior of each specimen is almost similar. The curves tend to overlap, especially for the specimens with infill of 100% and 75%. The overlap is almost identical especially for the elastic area of the curves, differences being noticed only in the plastic area. These can be explained by the fact the manufacturing problems of the specimens—from the raw material to the deposited material. These results can be corroborated with the results presented in Appendix A, where the specimens with increased infill values display a tendency towards similar behavior.

The deviations of the results for each set are calculated by means of Equation (1):

$$P\% = (P_i - P_m)/P_i\% \quad (1)$$

where:

- P%—the difference between the specific value of a specimen and the average value of the specimens in the set, expressed as a percentage;
- P_i—the specific value of the considered specimen;
- P_m—the average value of a parameter in a set of specimens.

Table 6 presents the maximum deviations for all the sets:

Table 6. Maximum deviations from the average value for all the studied sets.

	Fm [%]	Rm [%]	Fp [%]	Rp [%]	E [%]	ε [%]
Max deviation	−6.91	−7.32	15.81	14.97	−14.89	19.89

The maximum deviations of the strength are recorded for specimens with 25% infill density. This result supports the inconsistency in the behavior of the material with a decreased infill value.

Having the results for the longitudinal direction, the specimens were machined transversally using the same parameter setpoints, however with unfavorable results—see the specimens in Section 3.1.2 for the transverse direction and in Section 3.1.3 for the thickness direction.

3.1.2. The Transverse Direction

Figure 6 presents the manufactured specimens before and after tensile testing. The best results from the previous tests were used as manufacturing parameters.

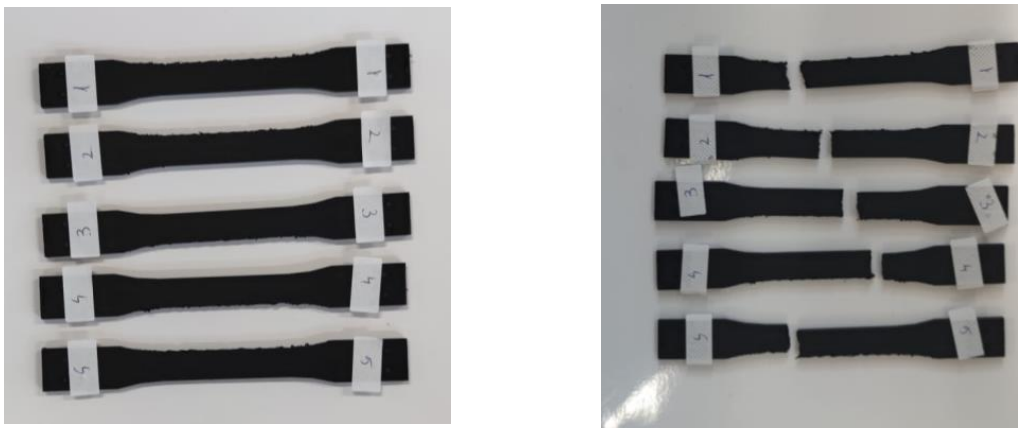

(**a**) (**b**)

Figure 6. Transverse Direction Tensile Specimens C_15_100: (**a**) Before testing; (**b**) After testing.

Figure 7 below shows that the curves are not overlapping completely; the failure is initiated in different points up to different strain values. These discrepancies are explained by the specimens' inconsistencies that are described in Section 3.2.

In this case, as presented in Table 7, for three out of the five specimens the material yielding starts from 9–10 MPa, compared to the other two where the yielding starts from values over 40 MPa. The failure occurs for Rm ranging from 41 MPa to 49 MPa. Strains at rupture recorded lower values compared to the specimens in the longitudinal direction, ranging from 1.00% to 1.80%.

Table 7. Transverse Direction Tensile Specimens Result—C_15_100.

Specimen	Fm [kN]	Rm [MPa]	Fp [kN]	Rp [kN]	E [GPa]	ε [%]
C_15_100_1_t	1.769	41	0.384	9	7	1.76
C_15_100_2_t	2.027	44	2.021	44	7	1.20
C_15_100_3_t	2.004	46	0.388	9	7	1.80
C_15_100_4_t	1.741	42	0.419	10	7	1.00
C_15_100_5_t	2.045	49	1.901	45	7	1.60

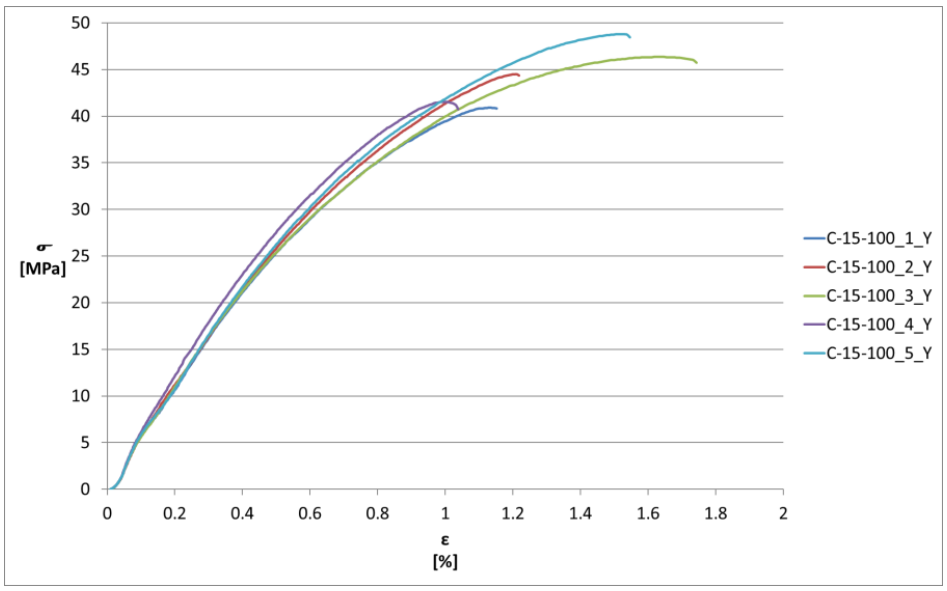

Figure 7. Transverse Direction Tensile Specimens results—Stress-Strain curves for C_15_100.

The discrepancies between these results can be explained by the fact that the specimens where the Rp is closer to the Rm value behave like brittle materials, whereas the others behave like ductile materials. These differences are related to carbon fiber consistency and arrangement in the matrix.

3.1.3. The Thickness Direction

Figure 8 presents the manufactured specimens before and after tensile testing. The best results from the previous tests were used as manufacturing parameters.

(**a**) (**b**)

Figure 8. Thickness Direction Tensile Specimens C_15_100: (**a**) Before testing; (**b**) After testing.

Figure 9 presents the results obtained for tensile specimens oriented by the thickness direction, in this case the inconsistency between specimens is clear: the stress-strain curves differ and failure occurs immediately. A reason for this result is the weak bondage between the layers, also asserted in [31]. Also, this alignment of parts on the printing plate is contrary to the recommendations found in literature based on that fact that increased tensile strength is obtained in the printing direction. In Figure 9 it can be observed that for specimen 3 the bondage of the layers is stronger compared to the rest of the specimens.

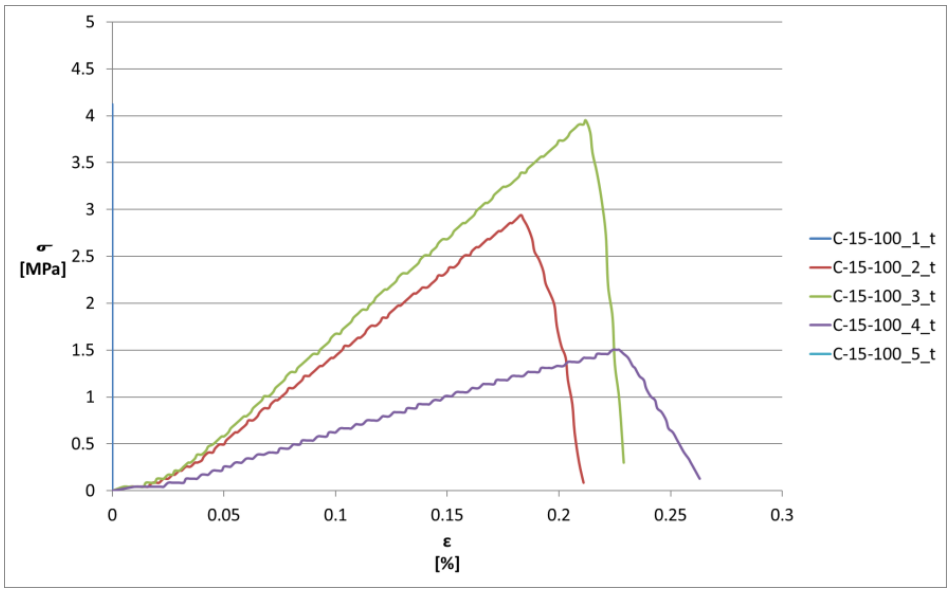

Figure 9. Thickness Direction Tensile Specimens results—Stress-Strain curves for C_15_100.

In Table 8 no values are recorded for specimens number 1 and 5 due to the fact that these specimens could not be fit between the grips for testing. Thus an average value could be calculated. Further on the following average values were used:3 tensile strength MPa, 1 MPa Yield Strength, 1 GPa Young's Modulus, and 0.23%strain at rupture. The results are necessary to offer a material description in all directions, i.e., to build the stiffness matrix in the hypothesis of an orthotropic material. These values are selected as an average for each type of result.

Table 8. Thickness Direction Tensile Specimens Result—C_15_100.

Specimen	Fm [kN]	Rm [MPa]	Fp [kN]	Rp [kN]	E [GPa]	ε [%]
C_15_100_1_t	0.192	4	0.099	2	-	0.30
C_15_100_2_t	0.137	3	-	-	2.94	0.21
C_15_100_3_t	0.184	4	0.045	1	1	0.23
C_15_100_4_t	0.070	2	-	-	1	0.26
C_15_100_5_t	-	-	-	-	-	-

Considering the presented results, achieving an ideal positioning of the part on the machine table represents a challenge.. The final utilization of the part should be known, as well as the load path that can appear in the assembly and the weak points in the structure, because the load path during operation is not singular and the risk of failure is increased. If a predominant uniaxial tensile loading appears in the structure, it is recommended to conduct material deposition in the part along the direction of load direction.

Another comparison can be made by the type of machine: with enclosure or without an enclosure, respectively. For a machine without an enclosure, as stated in [16], the best result is obtained for a thickness layer of 0.15 mm with an infill density of 100%. The tensile strength is 58 MPa. When using a printer with an enclosure with the same combination of parameter setpoints the tensile strength increases to 65.4 MPa. This can be explained by the fact that the enclosure preserves better the environmental temperature, the deposited material maintains its temperature for a longer period of time thus improving material bonding.

3.2. Defects—From Raw Material to Final Part

The differences in behavior can be explained by defects that appear from raw material to manufacturing. A "snow-ball effect" is generated because the raw material defects are transferred to the final part as manufacturing defects, affecting the part's functionality.

3.2.1. PET CF15 Raw Material Defects

PET CF15 raw material was studied under the microscope in order to check dimensional deviations, fiber orientation and arrangement in the matrix before utilization. Figure 10 below presents a section through the PET CF15 filament used in the research. The section shows deviations from the circularity, with several grooves at the edges. The darker areas visible in the cross-section indicate randomly scattered material voids and gaps. it can be noticed further that the fibers are oriented perpendicularly on the section, with some exceptions that are marked.

Figure 11 shows the same issues enhanced 100 times.

Figure 12 presents a longitudinal section of the filament, enhanced 100 times on the microscope. Material voids scattered randomly are also visible. This image offers a "map" of the studied section with fiber conglomerates and voids. This explains the unequal material distribution in the fiber and also in the studied specimens. Fibers are orientated mainly longitudinally in the filament. There are also fibers oriented randomly in the matrix, as confirmed by the findings reported in [11]. Visually fiber length varies between 50 and 200 μm, as concluded by analyzing the plots.

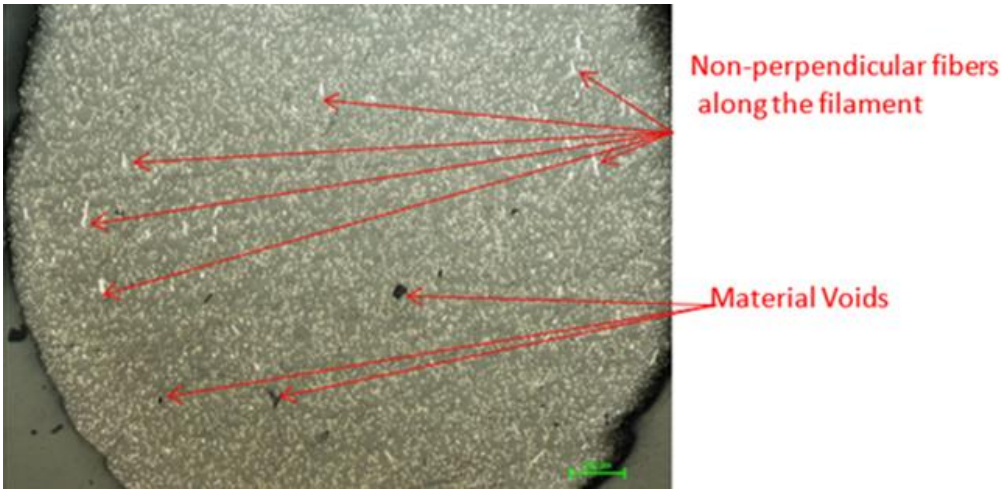

Figure 10. Ultrafuse PET CF15—Transversal view of the filament—Scale 50× (Scale length 200 µm) —Nikon T1-SM.

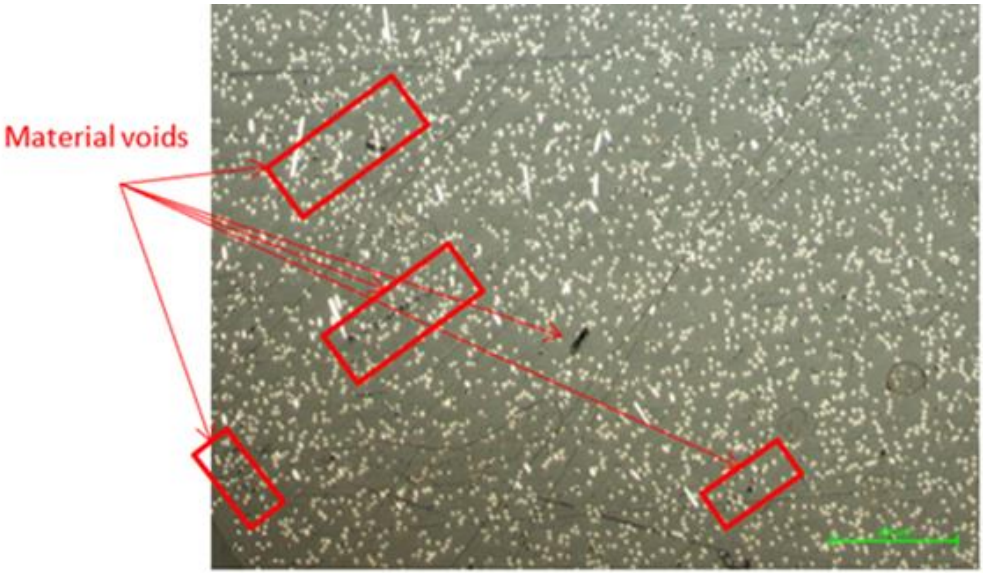

Figure 11. Ultrafuse PET CF15—Transversal view of the filament—Scale 100× (Scale length 200 µm) —Nikon T1-SM.

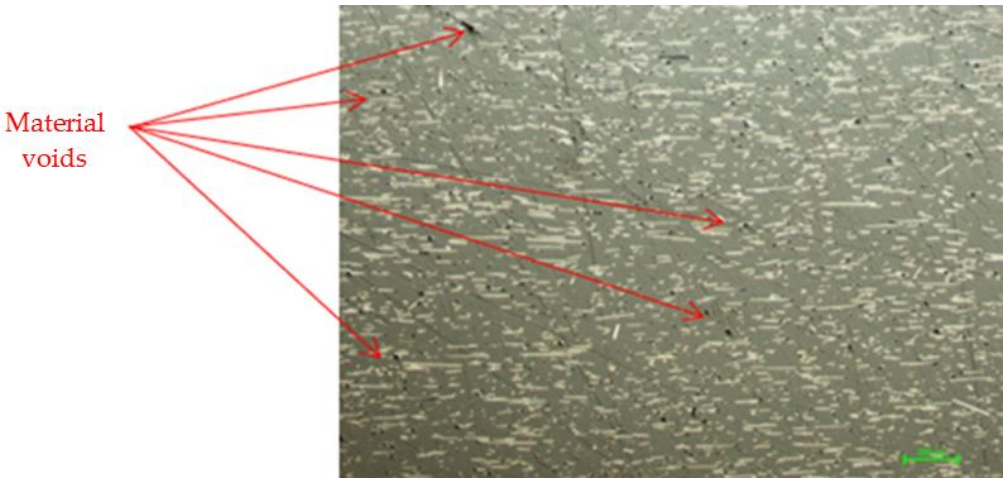

Figure 12. Ultrafuse PET CF15—Longitudinal view of the filament—Scale 100× (Scale length 200 µm) —Nikon T1-SM.

The results of the SEM analyses conducted on the filament are displayed in Figures 13–16. Figure 13 shows the longitudinal view of the filament at a scale factor of 350× and in Figure 14 shows the detailed view enhanced 600× of the area marked in Figure 13.

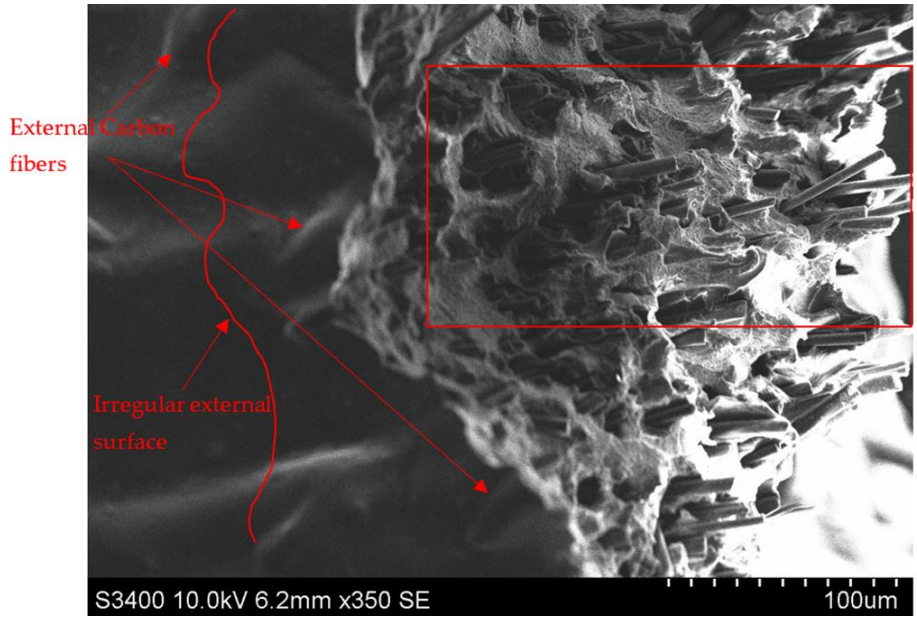

Figure 13. Ultrafuse PET CF15—Longitudinal view of the filament—Scale 350× (Scale length 100 µm) —Hitachi S3400N Type II.

Figure 13 shows the external surface of the filament which is irregular, some randomly oriented carbon fibers can be noticed on the external surface. Based on the orientation of the fibers in the rupture area it can be asserted that the main orientation of fibers is longitudinal. In the detailed view in Figure 14 areas without any carbon fiber are visible, circled red, as well as areas with fiber conglomerates. Both Figures 13 and 14 reveal areas around the fibers with micropores, accounting for the lack of adhesion of the fibers to the matrix. Figure 14 shows also the areas of fiber breakage., In the section through the filament voids are visible that bear the print of the pulled-out fiber.

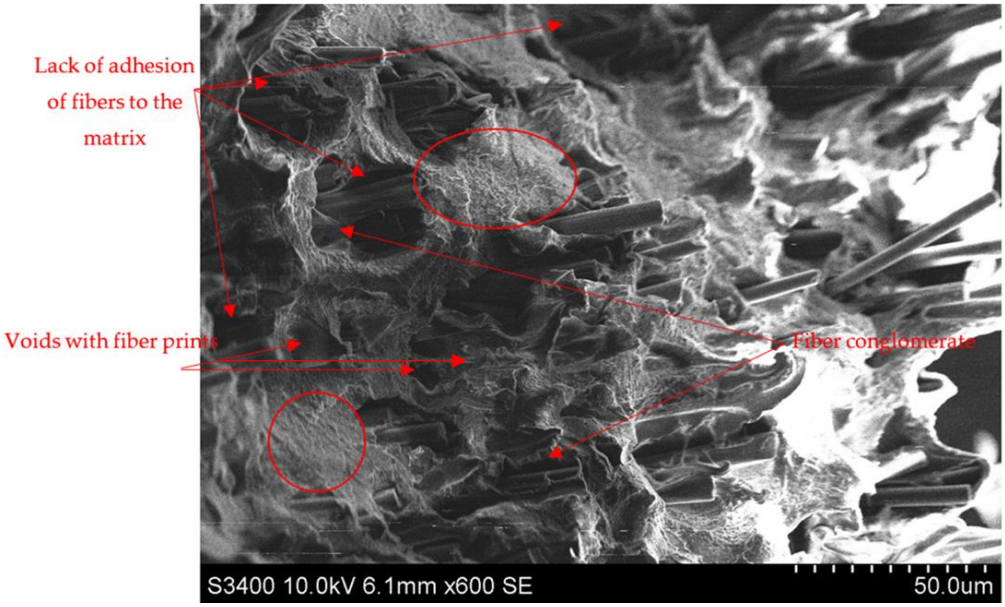

Figure 14. Ultrafuse PET CF15—Longitudinal view of the filament—Scale 600× (Scale length 50 µm) —Hitachi S3400N Type II.

Figure 15 shows a transversal view of the PET CF15 filament after SEM analysis. The 320× scaled image shows the increased number of voids of different dimensions. Only some of these are marked in the figure given the large amount of this defect. The same figure reveals several areas where fiber orientation deviates from the required one. In Figure 14 lower fiber density areas are marked with red circles, indicative of a random distribution of fibers.

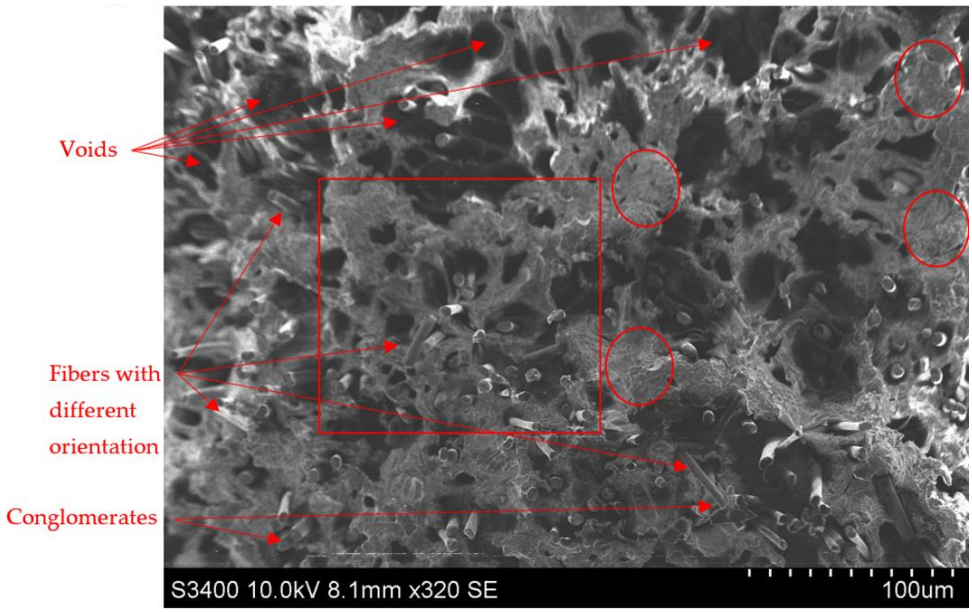

Figure 15. Ultrafuse PET CF15—Transversal view of the filament—Scale 320× (Scale length 100 µm) —Hitachi S3400N Type II.

Figure 16 shows the detail marked by the red box in Figure 15. The defects highlighted in Figure 15 are more visible, resulting from the voids that mark the poor adhesion of the fibers to the PET matrix. Also differently oriented fibers are more visible. In this detail image a complete fiber is visible, as well as an increased area without fibers marked with a red ellipse. Carbon fiber conglomerates are also visible confirming an irregular distribution of fibers in the raw material.

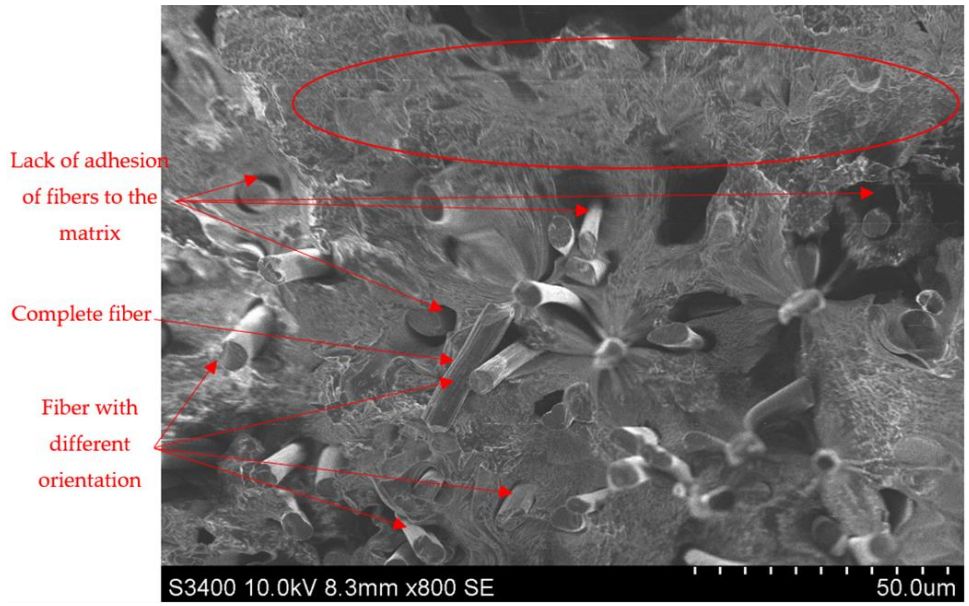

Figure 16. Ultrafuse PET CF15—Transversal view of the filament—Scale 800× (Scale length 50 µm) —Hitachi S3400N Type II.

Raw material issues are presented also in [32], where the studied material is PAHT-CF15 (Polyamide matrix with 15% Carbon Fibers from Innofil/Ultrafuse (BASF, Ludwigshafen, Germany). In this case the porosity is described during the manufacturing phase because the matrix is not adhering completely to fibers, resulting in material voids.

3.2.2. PET CF15 Tensile Specimen Manufacturing Defects

The defects mentioned in the previous subsection influence the characteristics of the final parts that depend also on the machine functionality, the manufacturing parameters and the state of the environment. All the tested specimens were visually inspected by means of a microscope, in order to identify the manufacturing issues caused by the previously mentioned factors.

Figures 17–35 present the identified manufacturing issues of the tested specimens. Material gaps were identified in all specimens, as presented in [24]. FEM validation of the tests is difficult due to unpredictable manufacturing issues. The volume of manufacturing defects is higher in specimens with a lower infill density of 25%, confirming the geometric instability mentioned in Section 1. It also offers an explanation for the results obtained for tensile testing, namely the increased number of defects in the considered parts. Also, because of material gaps, the differences in failure of parts with 100% infill are explained by their distribution and volume.

In Figure 17 a region is highlighted where the deposited material is not bonded, resulting in an area with material inconsistency. Also, due to the gap, the material deposited in its vicinity tends to be affected by slippage resulting in a cross-section of variable area, highlighted by the red polyline in Figure 17.

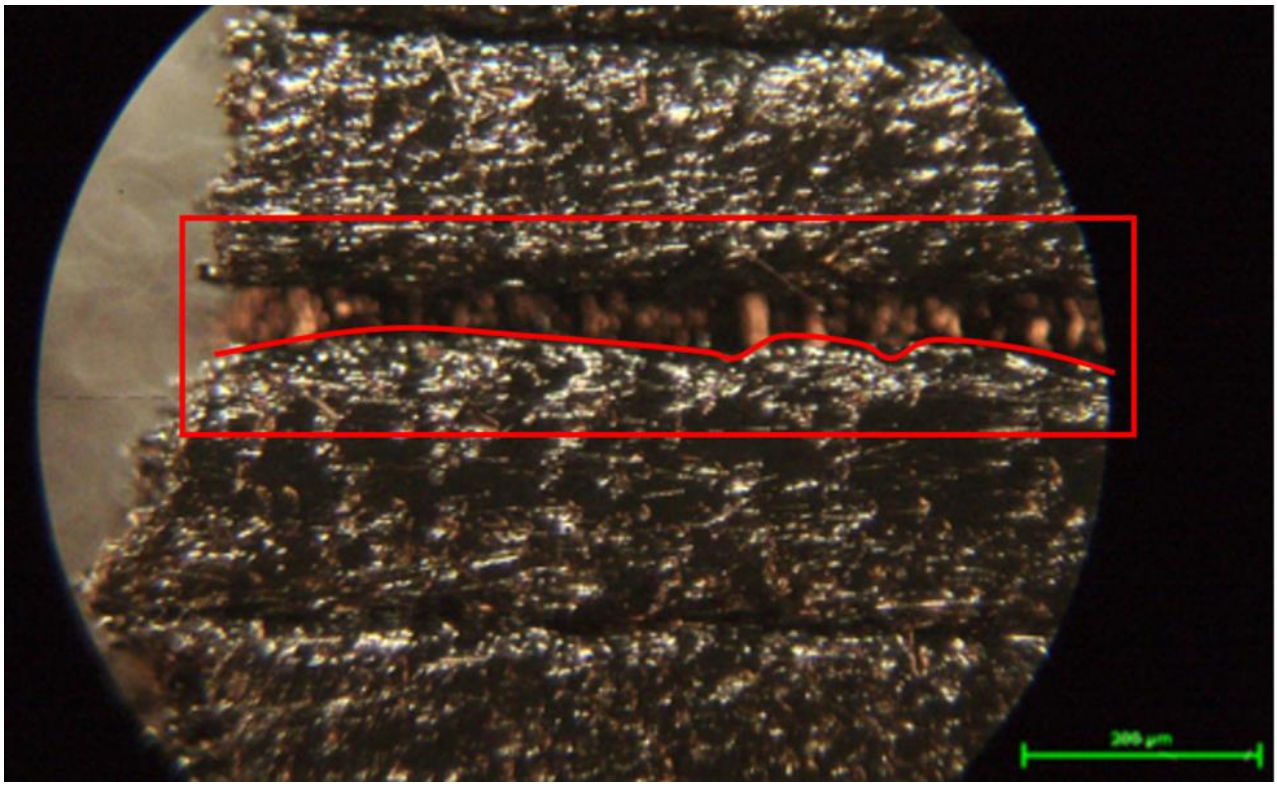

Figure 17. Specimens—Manufacturing defects—Voids between the layers (Scale 100×)—Scale length 200 µm—Nikon T1-SM.

Figure 18 shows another case of not bonded material in a specimen obtained by material deposition in the thickness direction. The deposited material from the infill area is not adhering to the shell causing gaps.

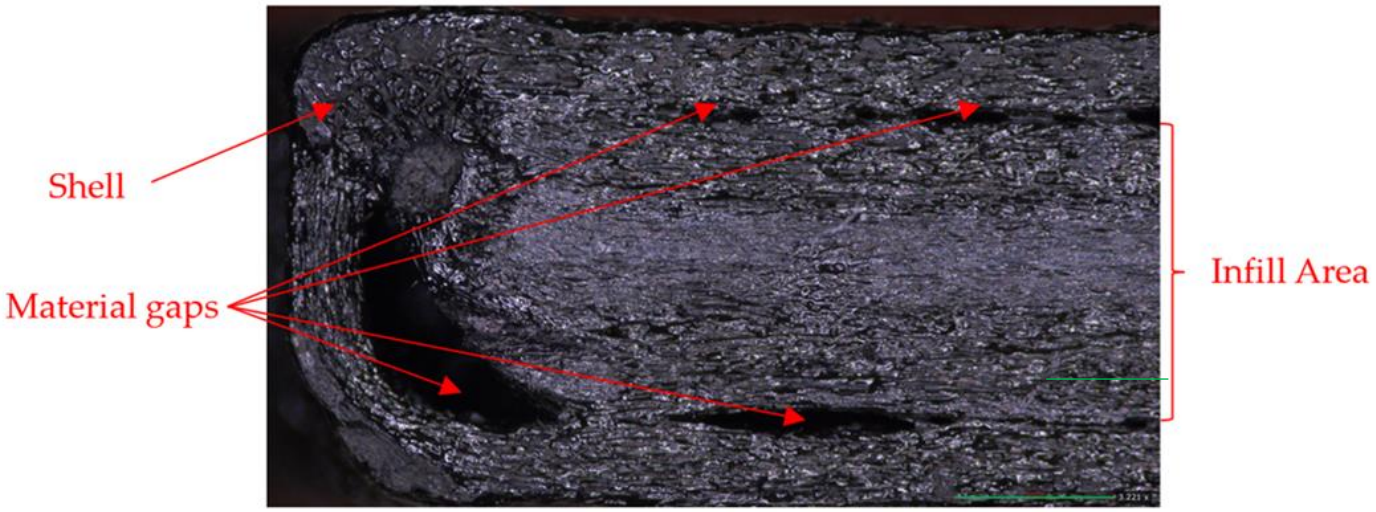

Figure 18. Specimens—Manufacturing defects—Voids between the layers (Scale 50×—Scale length 1 mm)—Emspira 3, Leica.

In Figure 19 an area is highlighted where the material is not deposited equally. The layers in the vicinity of the variable width raster have defined edges. Also, the resulted surface is not smooth due to some carbon fibers. The matrix is visibly darker and the fibers whiter, oriented along the direction of material deposition.

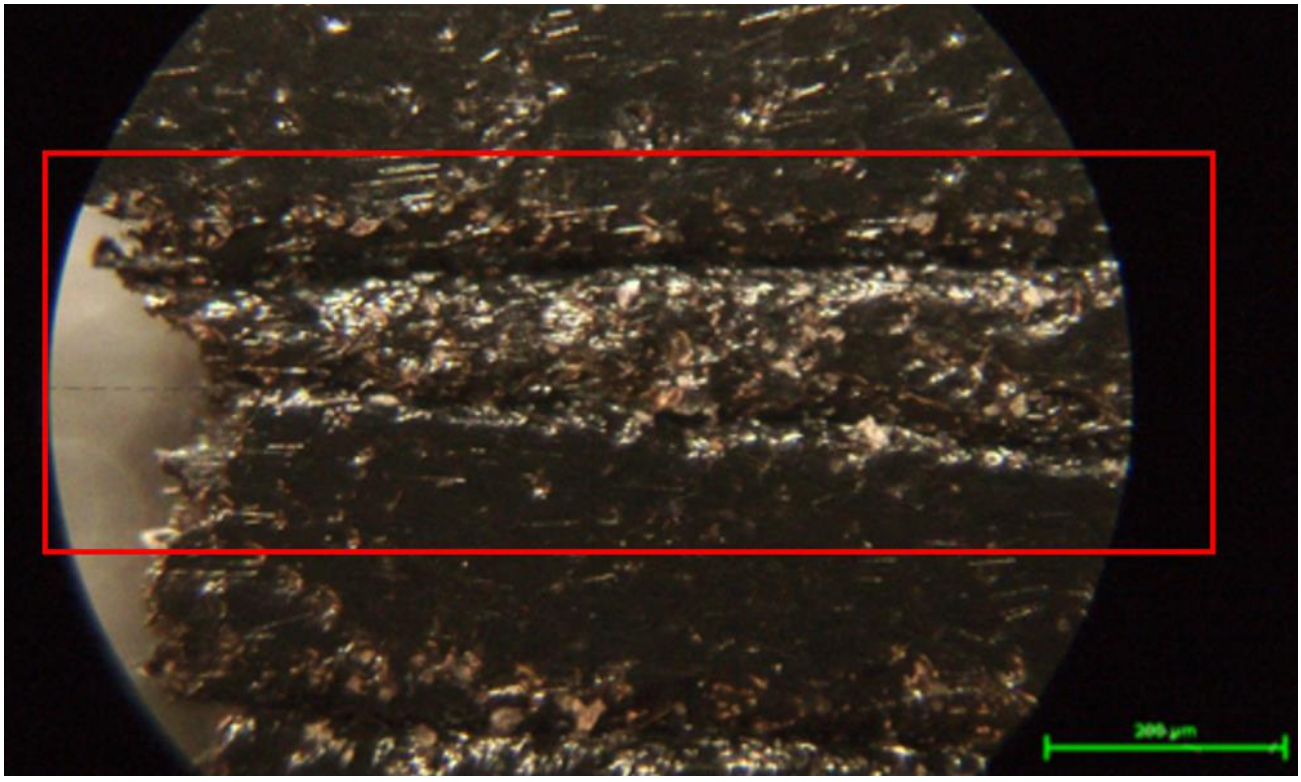

Figure 19. Specimens–Manufacturing defects–Unequal layer thicknesses (Scale 100×)–Scale length 200 µm—Nikon T1-SM.

In Figure 20 the areas are highlighted where the layers lack adhesion., The rupture during tensile tests is initiated in this area. Also, layer 1 is narrower than layer 2.

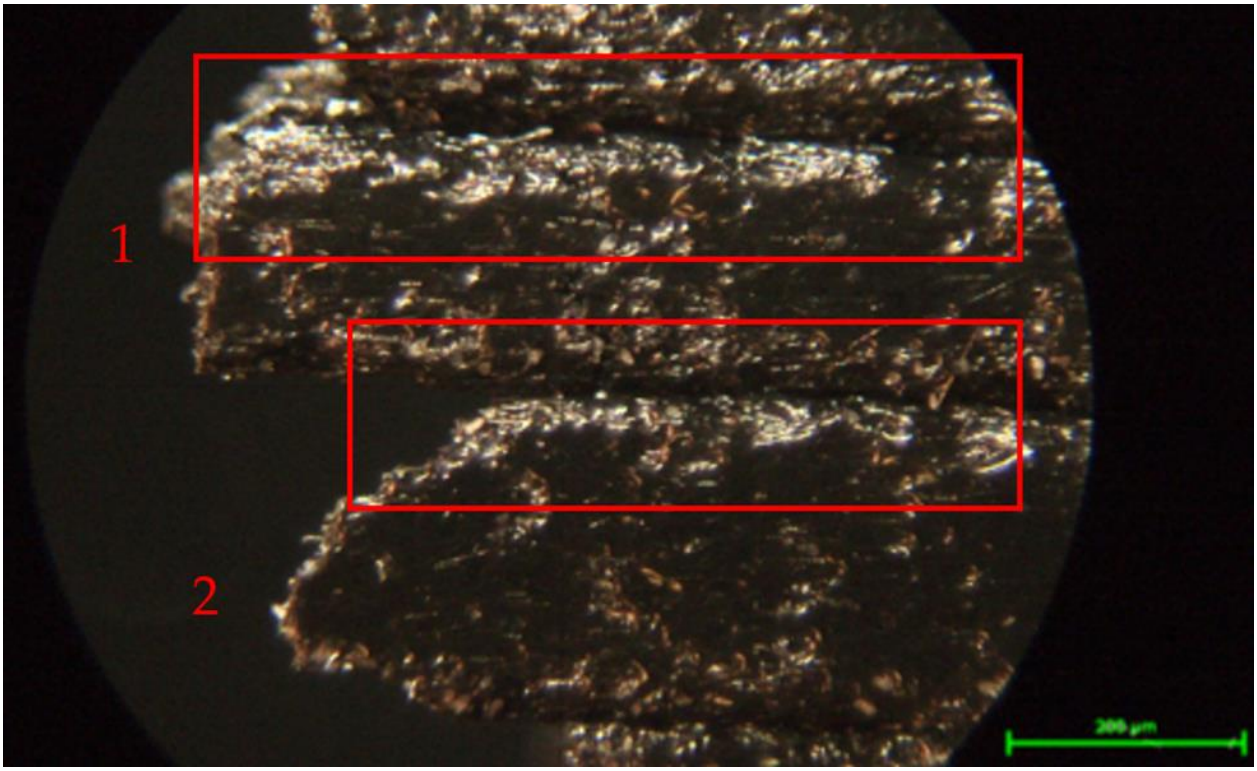

Figure 20. Specimens–Manufacturing defects–Lack of adhesion between the layers (Scale 100×)–Scale length 200 µm–Nikon T1-SM.

In Figure 21 an area of variable layer thickness is highlighted. This type of defect can be due to a variable flow rate that causes a material conglomerate followed by an area of lesser material deposition.

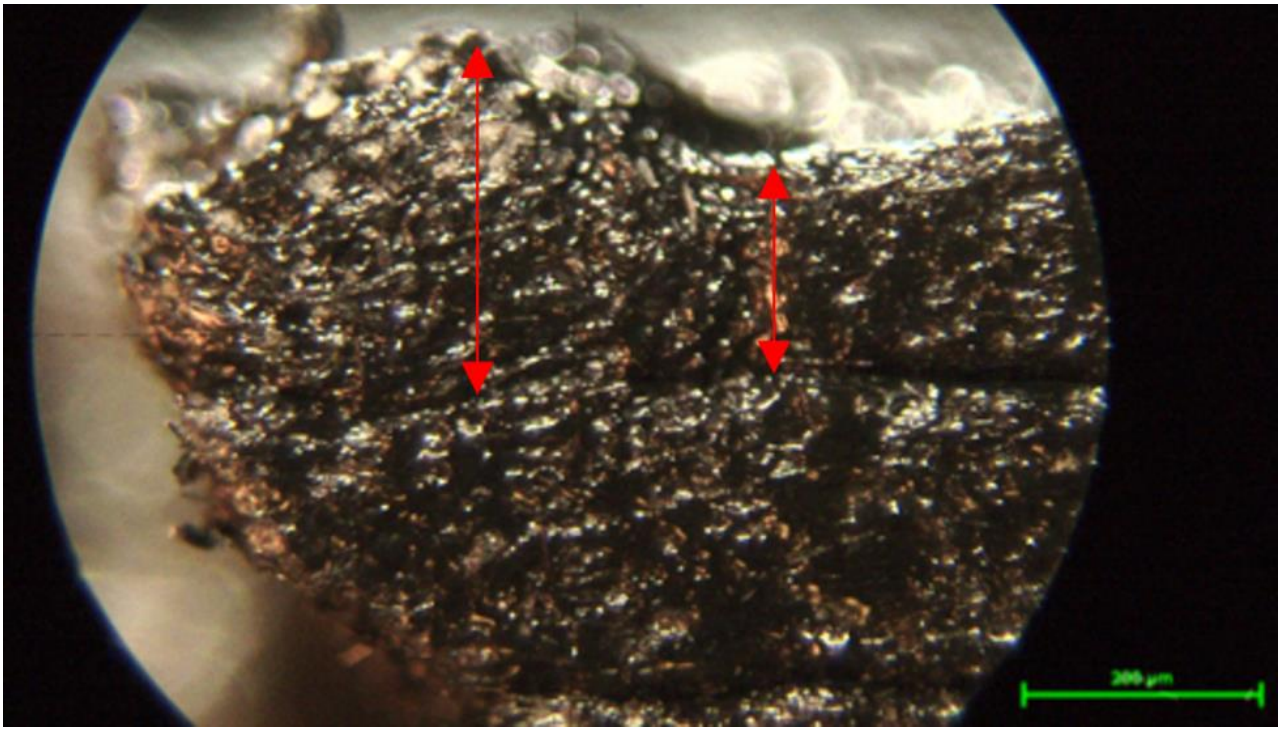

Figure 21. Specimens–Manufacturing defects–Non-constant thickness (Scale 100×)–Scale length 200 µm–Nikon T1-SM.

In Figure 22 an area is highlighted where a material conglomerate is deposited between the layers, causing a smaller width of the upper layer. Here the width of the specimen is different due to the layer on the left side of the highlighted region.

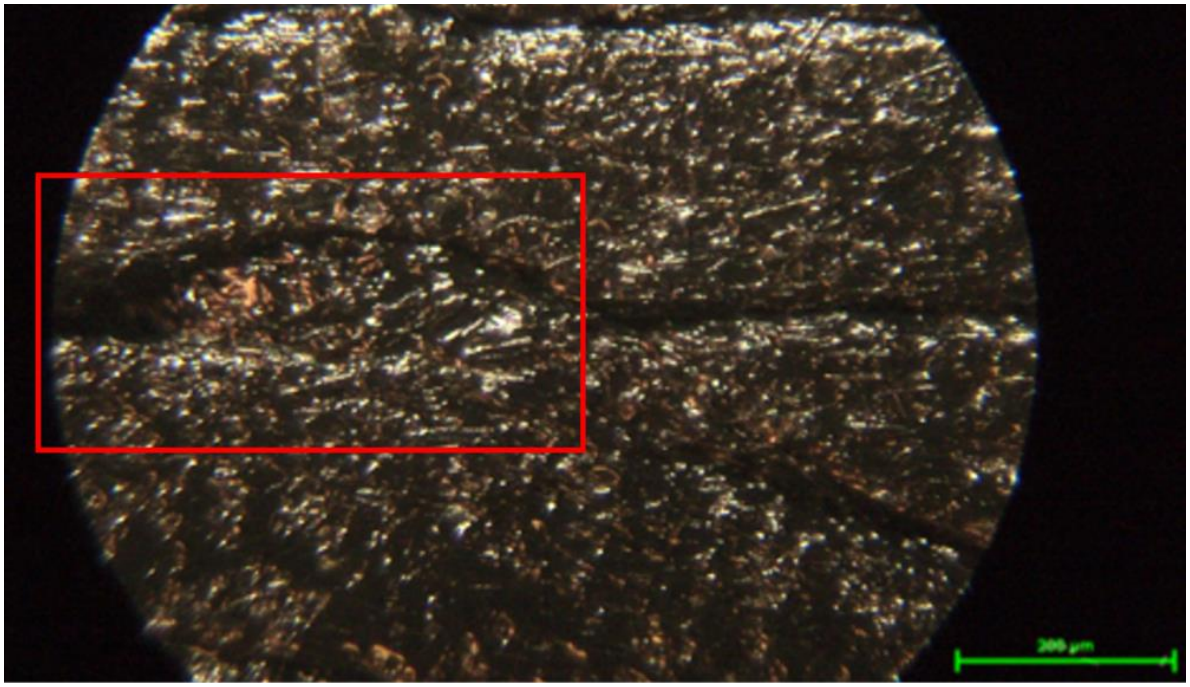

Figure 22. Specimens–Manufacturing defects–Material conglomerate (Scale 100×)–Scale length 200 µm–Nikon T1-SM.

In Figure 23 the highlighted region displays a faulty material deposition that fails to follow the normal direction of manufacturing. Thus the load path is affected leading to a maximum tensile load in the direction of material deposition.

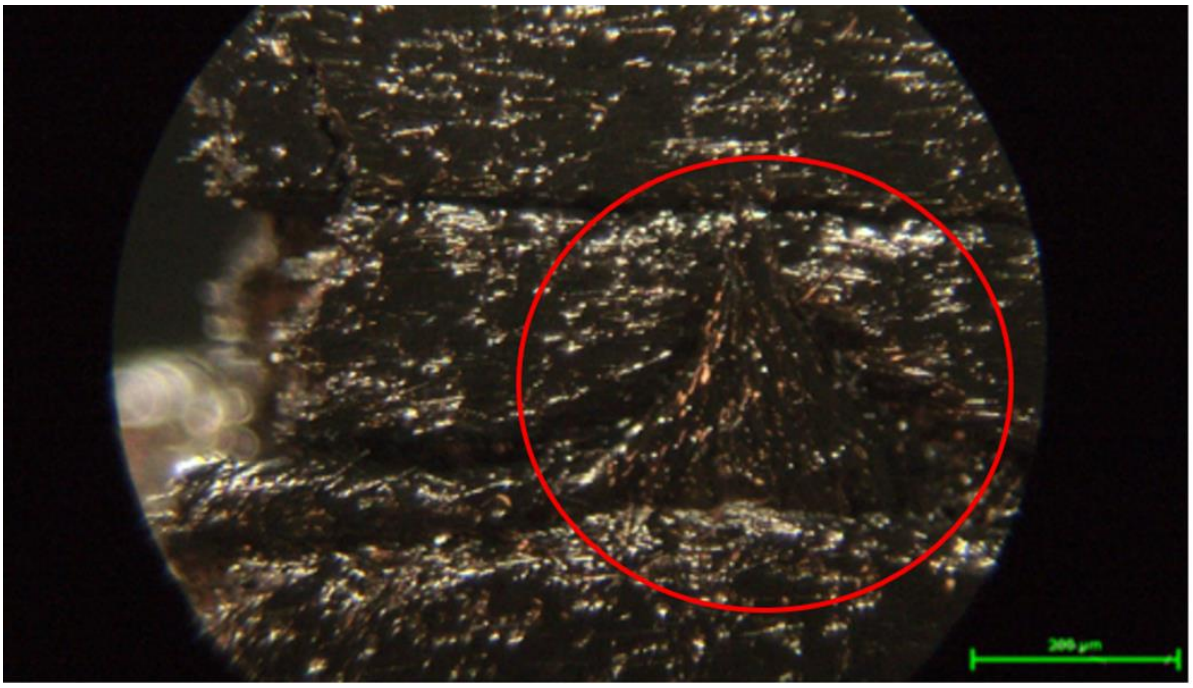

Figure 23. Specimens–Manufacturing defects–Inadequate material deposition (Scale 100×)–Scale length 200 µm–Nikon T1-SM.

Figure 24 shows lack of material in the specimen, causing material inconsistency. This defect occurred near the tensile failure area, leading to breakage in this region.

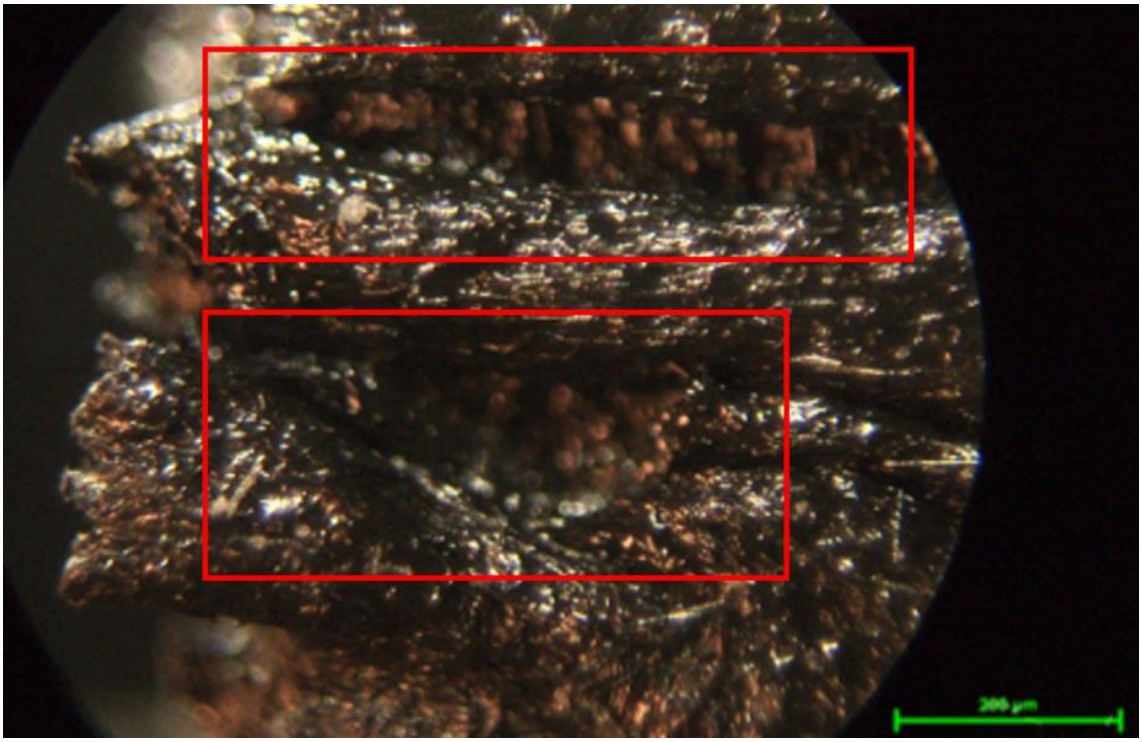

Figure 24. Specimens–Manufacturing defects–Material voids (Scale 100×)–Scale length 200 µm–Nikon T1-SM.

Figures 25 and 26 show cross-sections of the specimens with material void that cause delamination as a failure mode during the tensile testing.

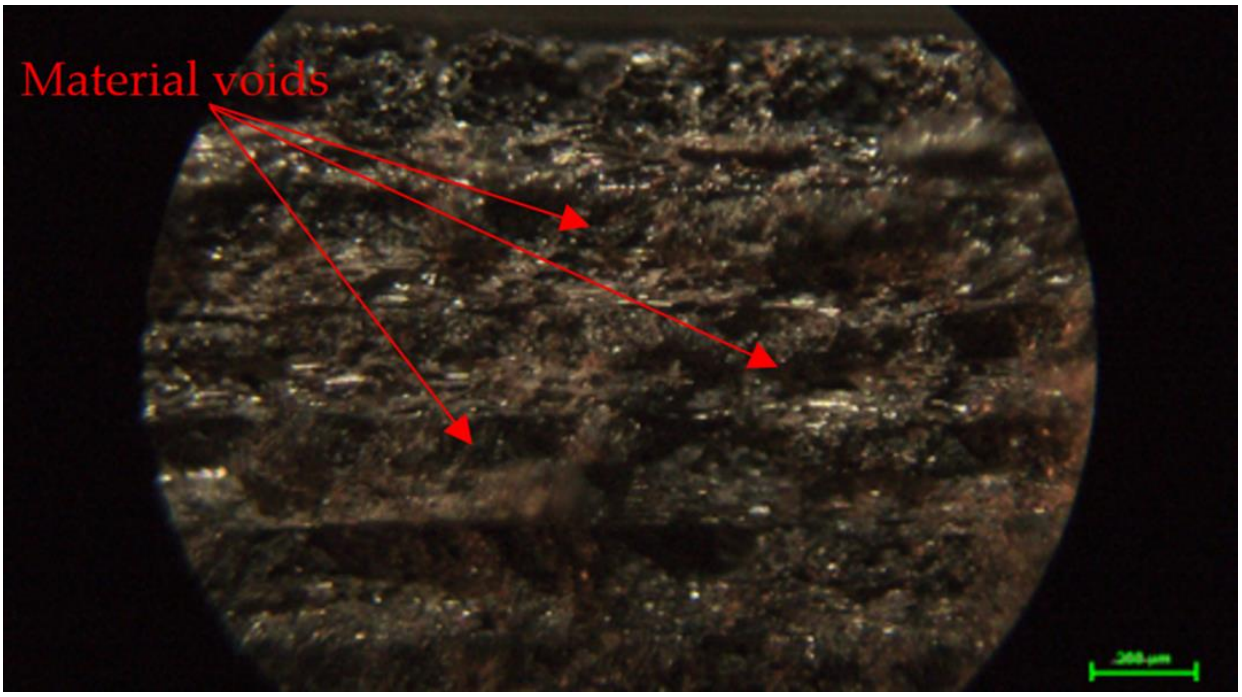

Figure 25. Specimens–Manufacturing defects–Material voids (Scale 50×)–Scale length 200 µm–Nikon T1-SM.

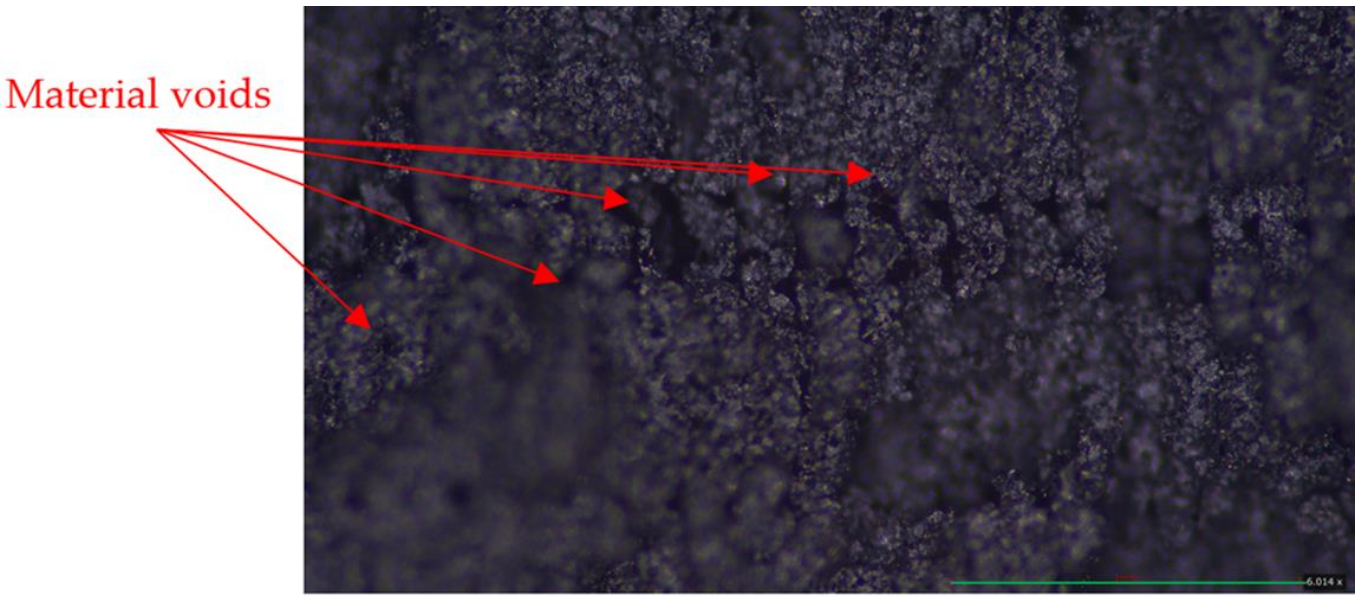

Figure 26. Specimens–Manufacturing defects–Material voids (Scale 100×–Scale length 1 mm)—Emspira 3, Leica.

Figure 27 shows a specimen edge of inadequate geometry.– After manufacturing, the deposited material fails to follow the ideal geometry. The higher material flow rate in this area causes the depositing of a larger amount of material.

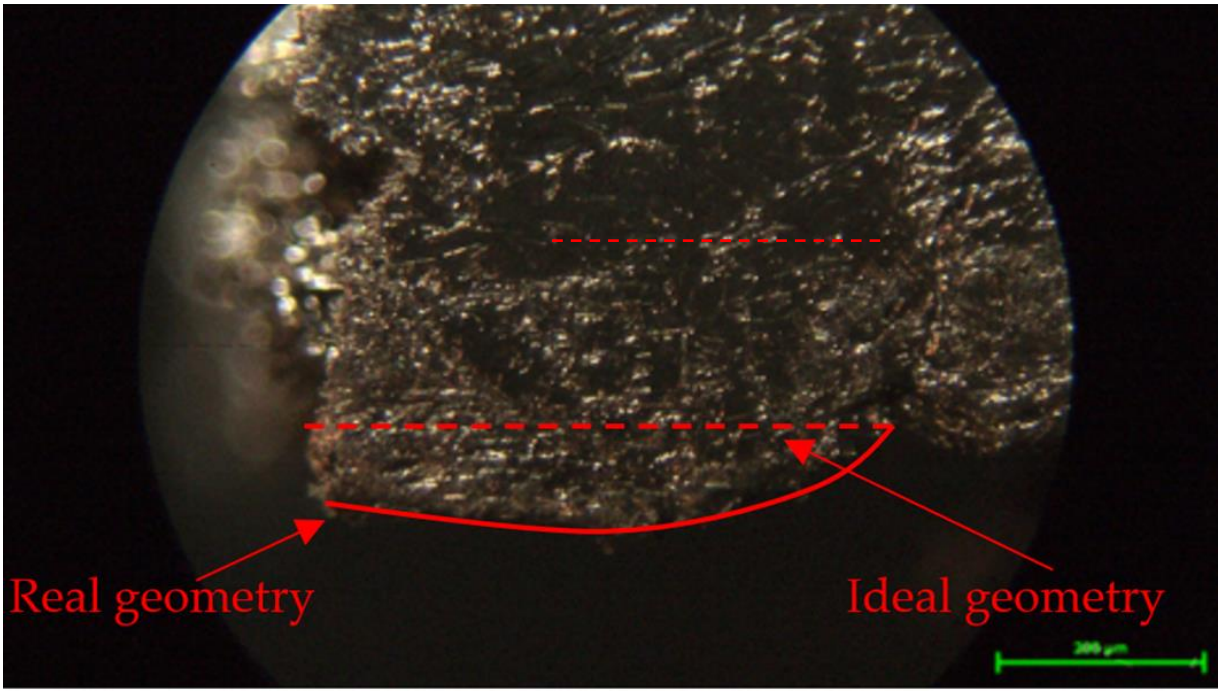

Figure 27. Specimens–Manufacturing defects–Inconsistent geometry (Scale 100×)–Scale length 200 µm–Nikon T1-SM.

Figure 28 shows a specimen with a lower infill density. The weak bonding of the infill layer is highlighted. This defect causes an inadequate load path, and failure is initiated in this area.

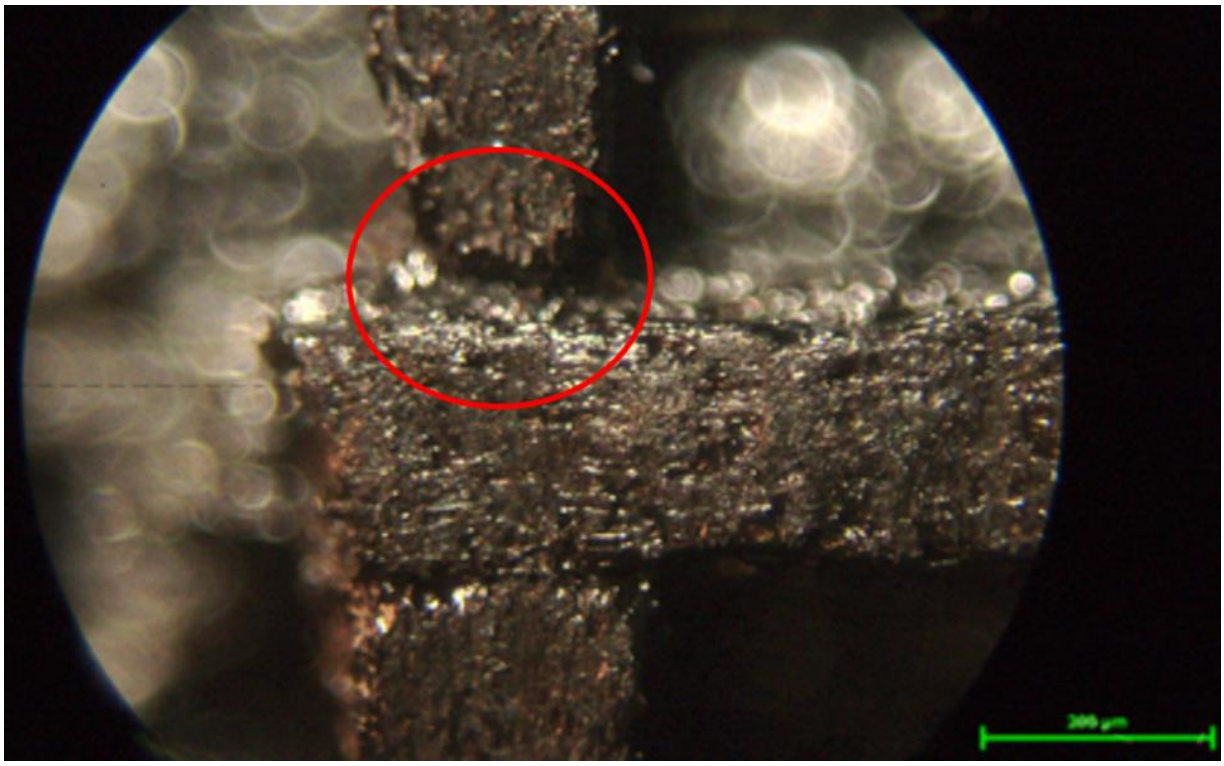

Figure 28. Specimens–Manufacturing defects–Weak bonding at the junction of the infill layer (Scale 100×)–Scale length 200 µm–Nikon T1-SM.

Figure 29 highlights the "stair-effect" that occurs at dimensional variation.. The defect appears in the area of variable width, being limited to the region held by the grips and the region used for tensile analysis. This is more visible in thicker layers.

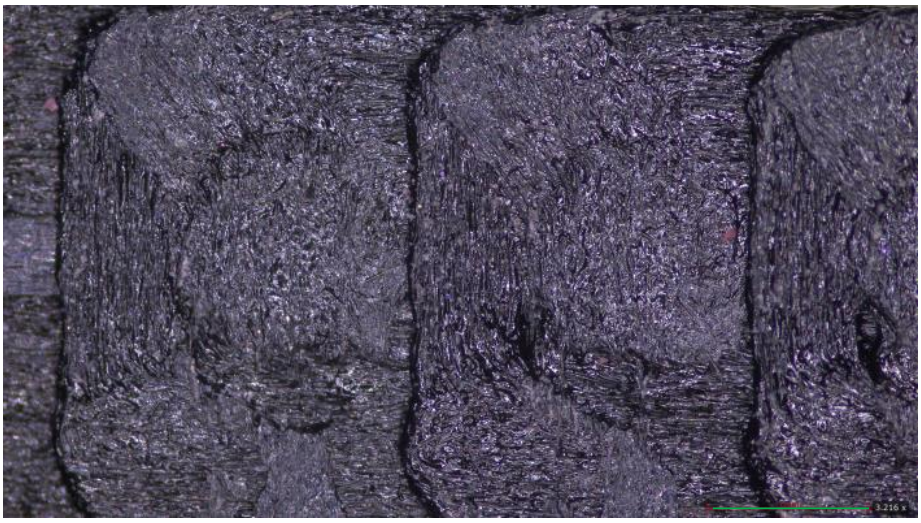

Figure 29. Specimens–Manufacturing defects–"Stair effect" (Scale 50×–Scale length 1 mm)–Emspira 3, Leica.

Figure 30 refers to the same cross-section. The layers do not overlap 100%. The profile of the offset layers follows the red polyline instead of a desired straight line. This defect is more visible in specimens manufactured in the thickness direction.

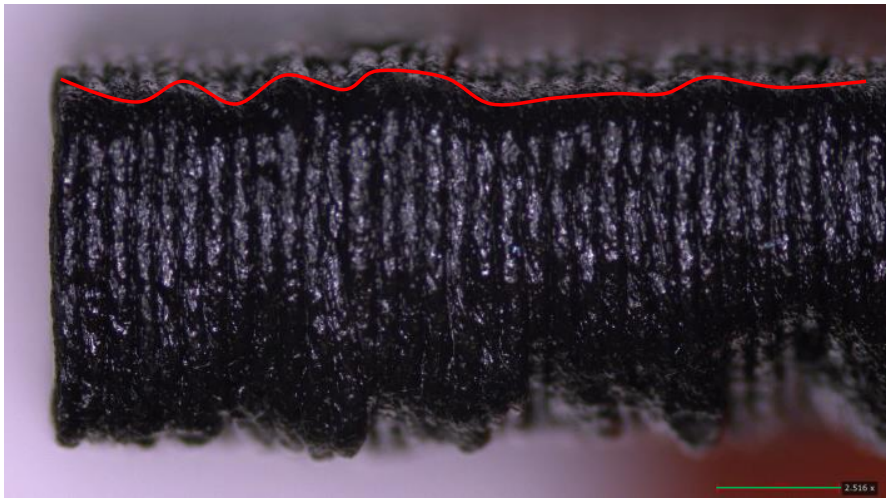

Figure 30. Specimens–Manufacturing defects–Offset layers (Scale 50×–Scale length 1 mm)–Emspira 3, Leica.

For specimens with an infill density of 75% or 25% in Figure 31 it can be observed that the unsupported layers tend to flow until the material sets, affecting the internal structure of the specimen. This effect is more visible for specimens with a lower infill density. The straight line in Figure 31 represents the ideal geometry of the specimen. The red rectangle highlights the set material after flowing.

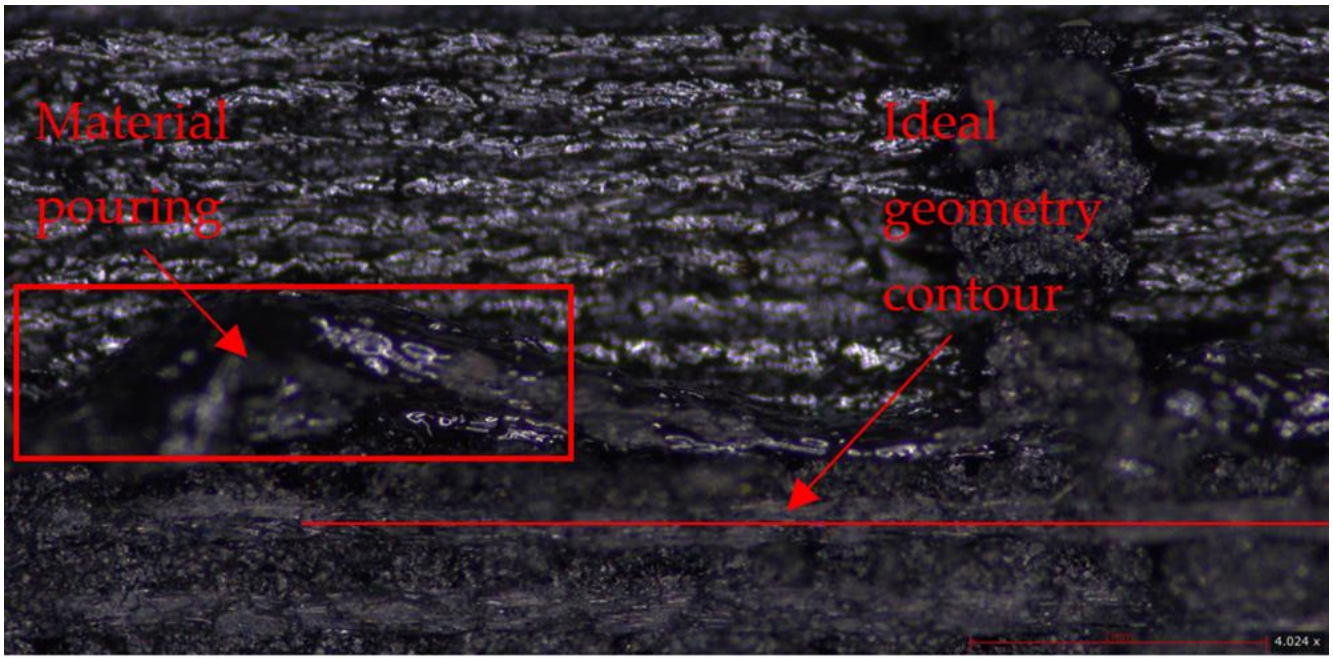

Figure 31. Specimens–Manufacturing defects–Material flowing (Scale 75×–Scale length 1 mm)–Emspira 3, Leica.

Figure 32 shows a SEM image of various manufacturing defects, such as deficient inter-layer adhesion and areas with visible carbon fiber dislocation from the PET matrix. The same plot shows the failure area after tensile testing, where the main failure mode is delamination. The red box in Figure 32 marks a detail that is presented in Figure 33. This is an area of inadequate material deposition that does not follow the direction of the nozzle movement.

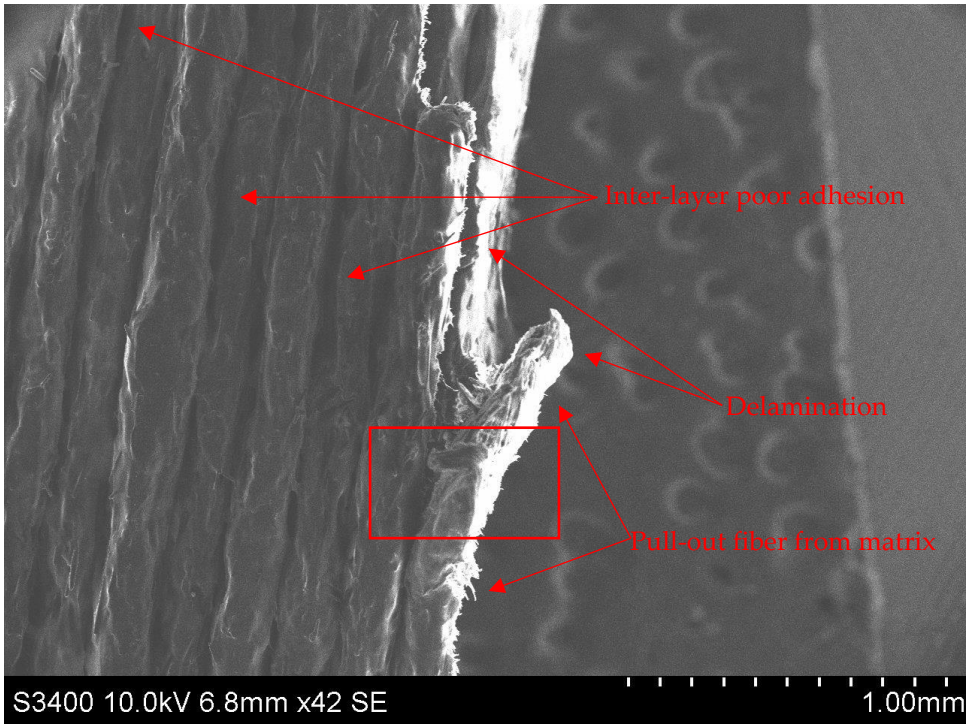

Figure 32. Specimens–Manufacturing defects–Various defects (Scale 42×–Scale length 1 mm)–Hitachi S3400N Type II.

In Figure 33 shows the area of deficient material deposition. An increased distance between the adjacent layers can be observed. Also on each layer material voids and fibers dislocated from the PET matrix are visible.

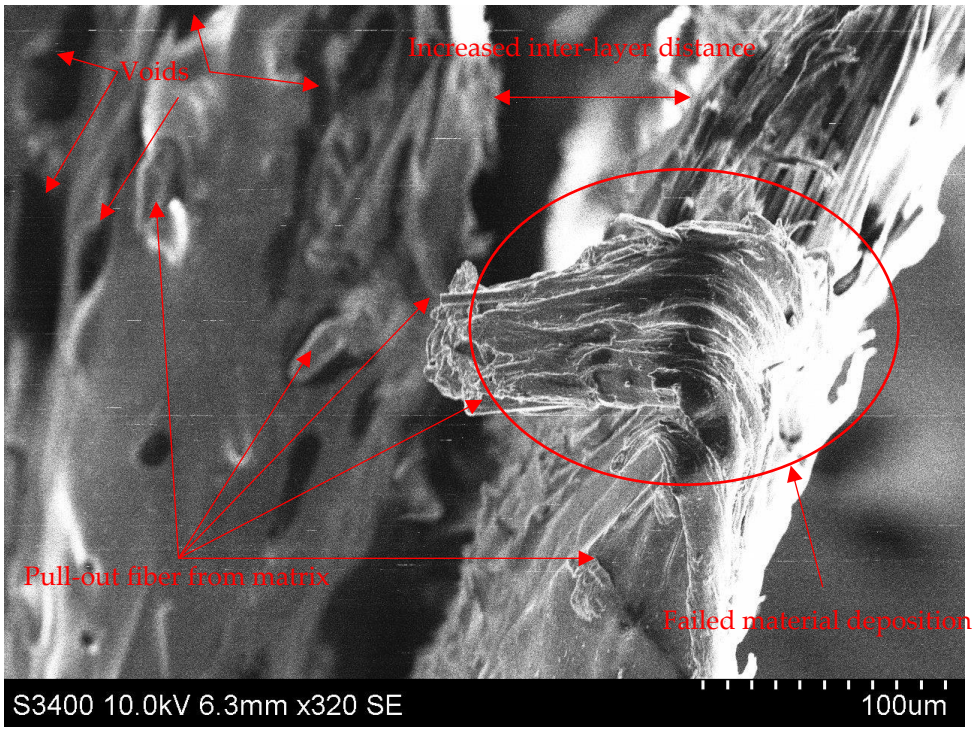

Figure 33. Specimens–Manufacturing defects–Various defects (Scale 320×–Scale length 100 µm)–Hitachi S3400N Type II.

Figure 34 shows a random inter-layer area which is irregular and also has material voids. The randomly oriented carbon fibers are also visible. The red box marks the area detailed in Figure 35.

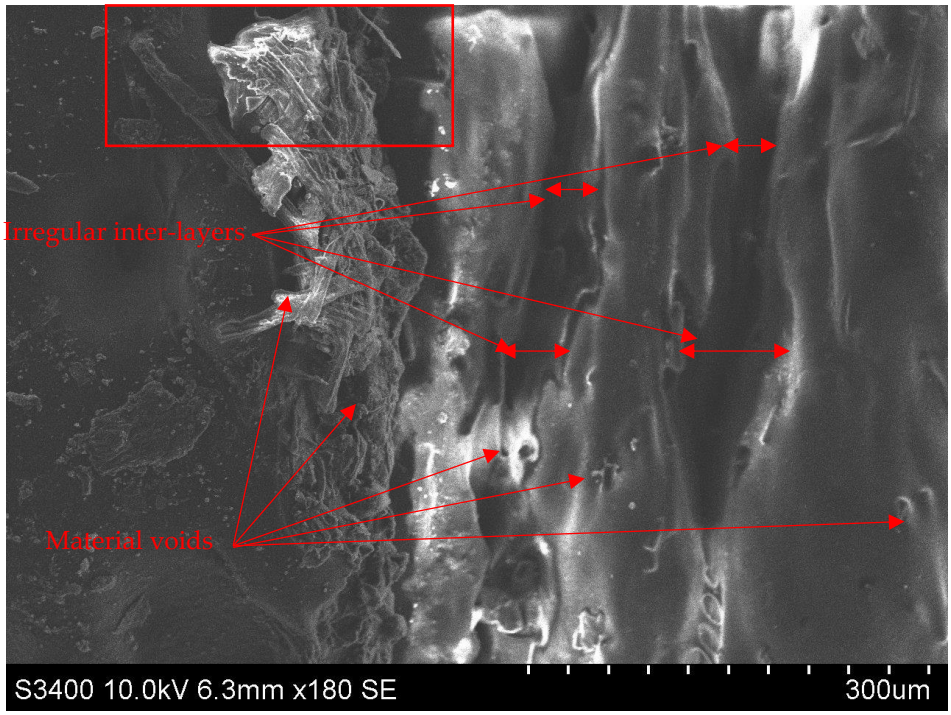

Figure 34. Specimens–Manufacturing defects–Various defects (Scale 180×–Scale length 300 µm)–Hitachi S3400N Type II.

Figure 35 shows an area with voids of different dimensions, with fibers of different orientations dislocated from the matrix. The variable inter-layer distance it is also visible.

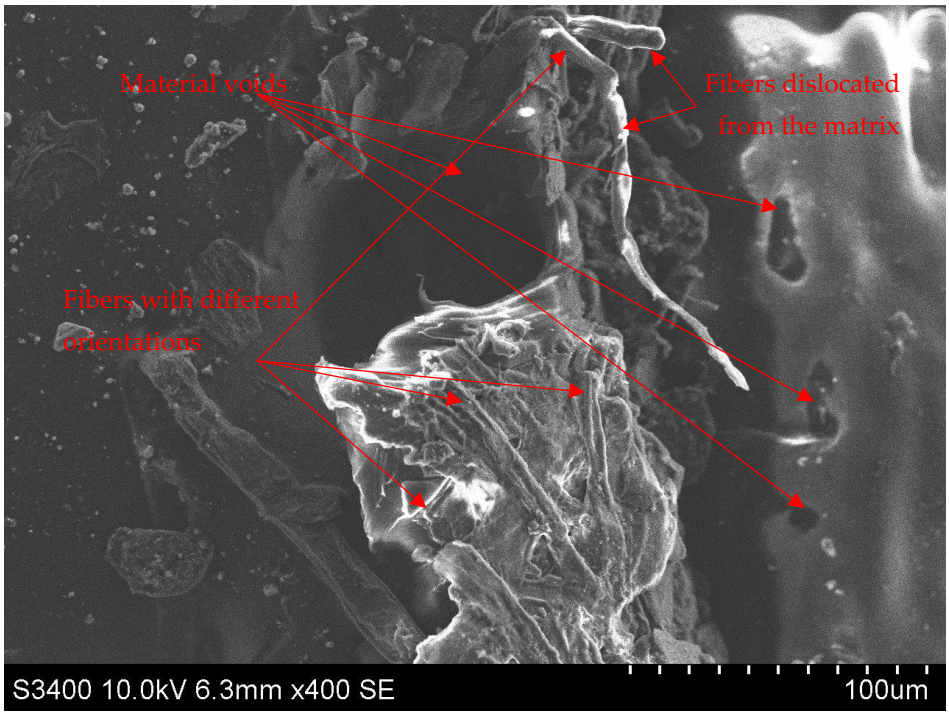

Figure 35. Specimens–Manufacturing defects–Various defects (Scale 400×–Scale length 100 µm)–Hitachi S3400N Type II.

As a conclusion, all manufacturing defects affect the mechanical properties because of material inconsistency that also affects the load path on the parts and, in the end, its performance. All specimens displayed material voids of different dimensions. Other possible defects cannot be predicted: varying fiber orientation, inconsistent inter-layer gaps or fiber dislocation from the matrix. It is recommended to test for certain failure types in order to define the material behavior, to determine a pattern and the optimal values for the main manufacturing parameters. The rest of the manufacturing parameters must be consistent, and the same machine should be used for printing.

3.2.3. PET CF15 Tensile Specimen Failure Modes

During the tensile tests different failure modes were identified that are caused also by the manufacturing defects. The most common failure issues identified during the visual inspection are presented in Figures 36–39.

Figure 36 shows a specimen after tensile testing, with fibers dislocated from the matrix. This type of failure can appear due to a weaker bonding between the matrix and the fibers, which can also cause fiber breakage.

Figure 37 shows a specimen after tensile testing where the failure is a delamination of the layers. This can be caused by manufacturing defects, such as material gaps or material conglomerates or weak bonding between the layers. Further it can be noticed that layer 2 is wider than its adjacent layers.

Figure 38 shows a specimen after tensile testing and its rupture area; further cracks near the failure area are visible.

Figure 39 shows a specimen after tensile testing and its rupture area; delamination is present and also cracks starting from the failure region and affecting almost all the layers in the vicinity of the rupture.

The main identified failure modes are delamination and material cracks, with fiber brakeage. Also in many cases the fibers were dislocated from the matrix, confirming the studies that assert that the matrix does not adhere completely to the fibers.

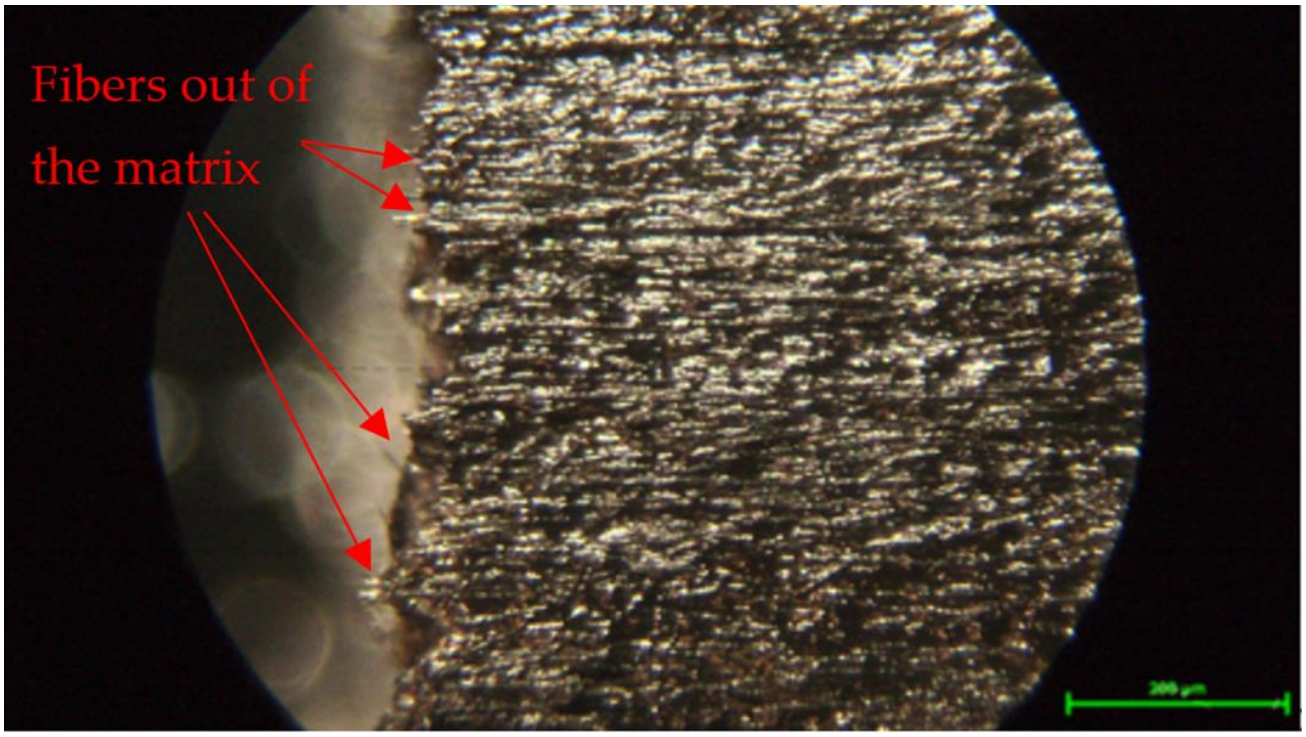

Figure 36. Specimens–Failure Modes–Fibers dislocated from the matrix and fiber breakage (Scale 100×)–Scale length 200 µm–Nikon T1-SM.

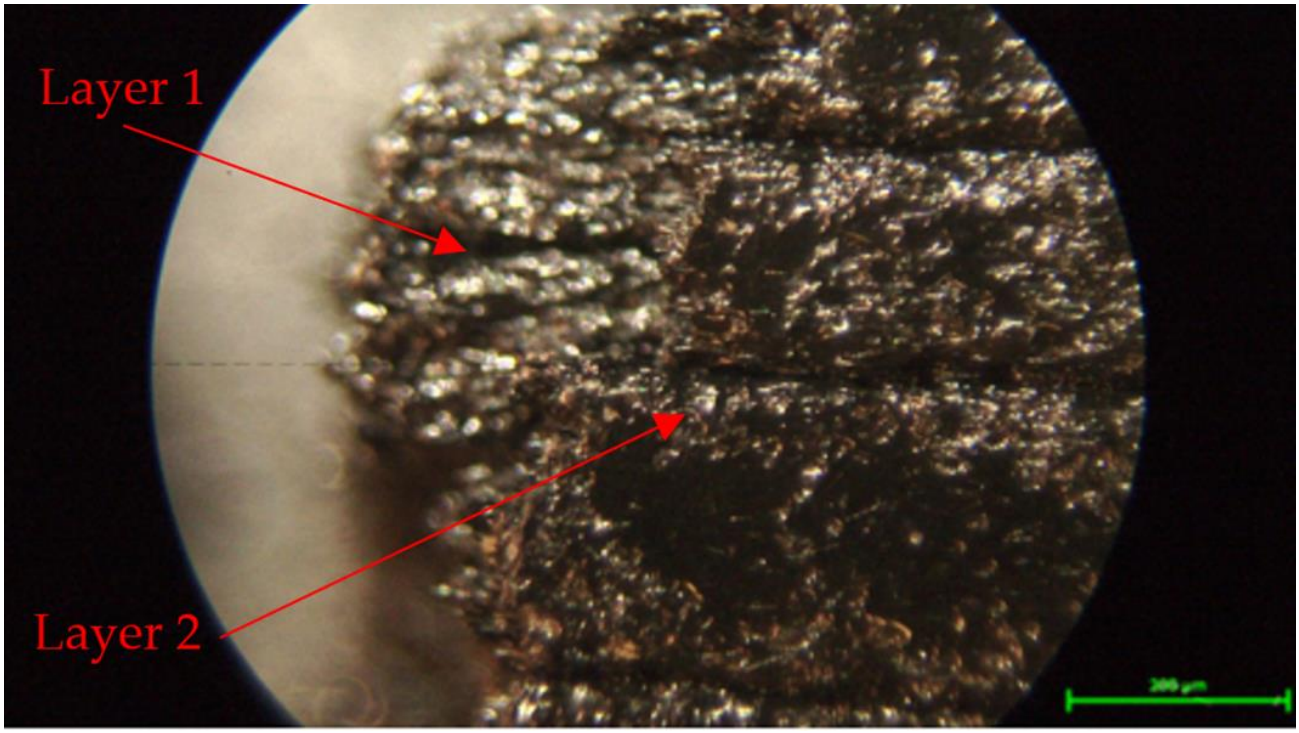

Figure 37. Specimens–Failure Modes–Delamination of the layers (Scale 100×)–Scale length 200 μm–Nikon T1-SM.

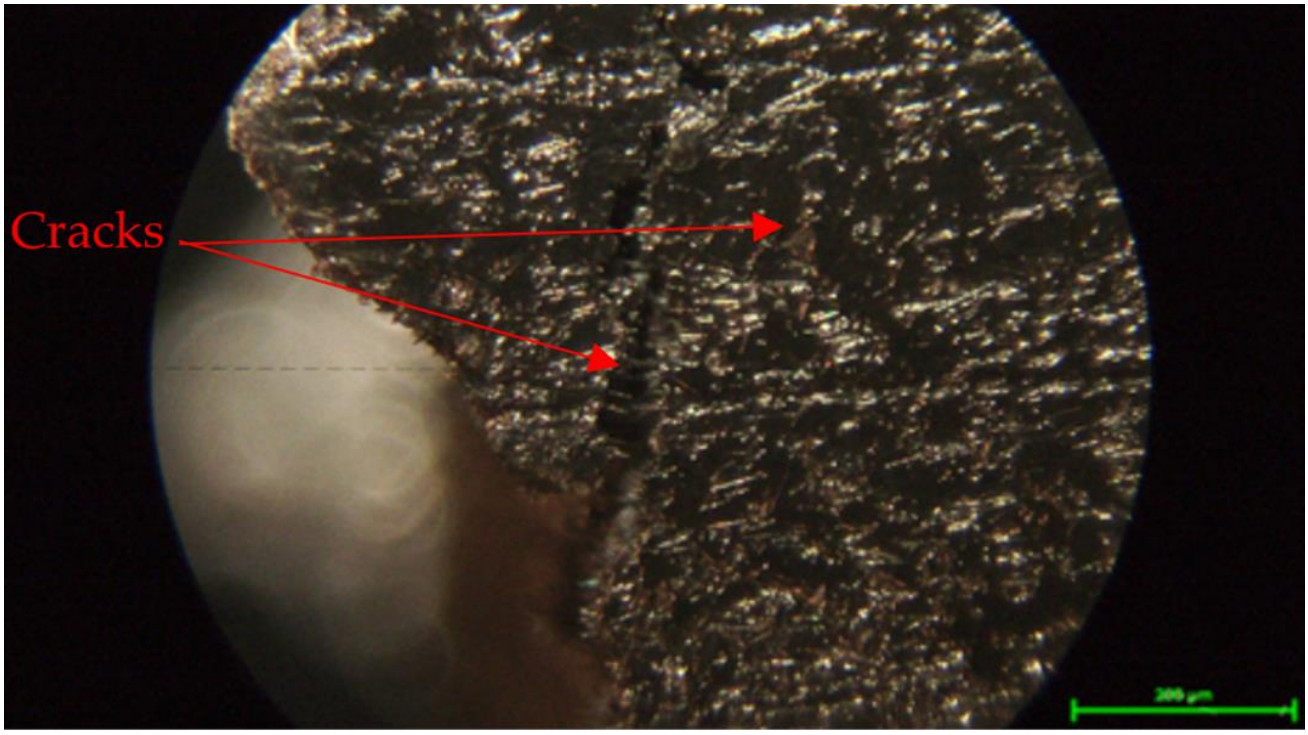

Figure 38. Specimens–Failure Modes–Cracks (Scale 100×)–Scale length 200 μm–Nikon T1-SM.

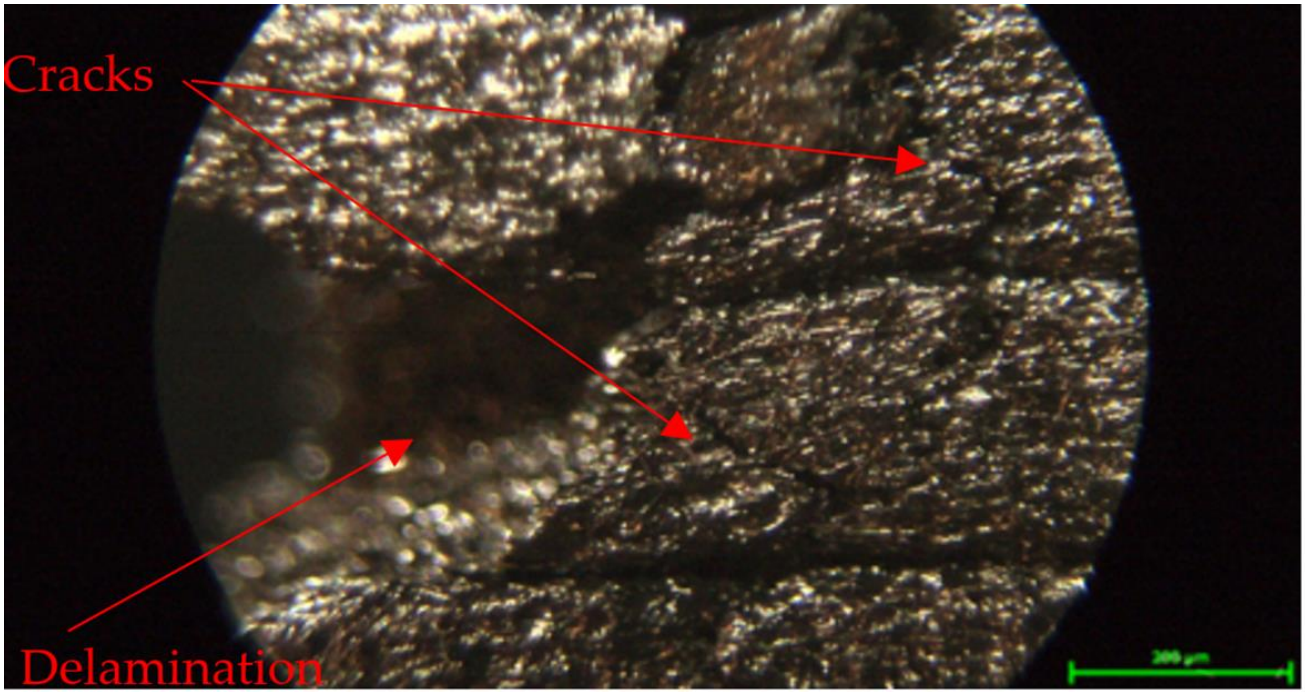

Figure 39. Specimens–Failure Modes–Delamination and cracks (Scale 100×)–Scale length 200 µm–Nikon T1-SM.

3.2.4. PET CF15 Tensile Specimen Dimensional Deviations

On each specimen the thickness and width of the area presumed to be the tensile section was measured. Subsequently the impact of specimen orientation on the geometrical parameters of the parts was determined as follows: for specimens with longitudinal material deposition all width measurements were greater than the nominal dimension of 13 mm; the measured width ranged from 13.21 mm to 13.82 mm. The thickness varied between 3.05 mm and 3.57 mm.

In specimens with transverse material deposition the measured thickness and width were greater than the nominal values. The thickness varied from 3.37 mm to 3.44 mm. The width ranged between 13.21 mm and 13.27 mm.

Material deposition along the transverse direction yielded thickness values ranging from 3.15 mm to 3.66 mm. The width was smaller than the nominal dimension of 13 mm, ranging from 12.82 mm to 12.98 mm.

These different values suggest the idea of a geometrical instability of the parts, even for specimens printed at the same time in sets of five. In [14] it is reported that in specimens with lower layer thickness the geometry varies less than in those with a greater layer thickness. Nevertheless, in this case, in addition to the aspects mentioned before, it can be asserted that part orientation and design also have a significant influence on its geometrical stability.

3.3. Design of Experiments

Statistical data processing and analysis of variance (ANOVA) were applied to the results of the tensile testing of the specimens with longitudinal material deposition. The mathematical model expressed by Equation (2) was obtained using Minitab 21. It can be used without further costs to expand and predict the outputs. Table 9 presents the summary of the model implemented in 45 iterations for the prediction of Rm. It used as input parameters the infill density (I) and the layer thickness (t), defined as independent variables, as well as the results of the tensile testing. Evidently Rm was the predicted dependent variable. The values of the independent variables and the running order are presented in Appendix C.

$$Rm = 67.7 + 0.2739\ I - 3.15\ t + 0.0653\ t^2 \quad (2)$$

Table 9. Summary of the polynomial equation model for the prediction of Rm.

S	R^2	Adjusted R^2	Predicted R^2
2.3268	94.08%	93.65%	92.85%

This model was selected due to the reasonable number of equation terms, it represents a strong relationship defined by the terms R^2, Adjusted R^2 and Predicted R^2 presented above. Their values also describe the correlation of the regression model, which in this case is high, over 90%. This result can be explained by the material inconsistency and the manufacturing defects identified during the tests.

Table 10 presents the ANOVA analysis of the regression model. Equation (2) includes only significant terms, corresponding to the Pareto Chart shown in Figure 32. This result was obtained after iterations where the terms with *p*-values exceeding 0.05 were removed from the mathematical regression model due to their inconsistencies.

Table 10. Analyses of Variance of the regression model.

Source	DF	Adjusted SS	Adjusted MS	F-Value	*p*-Value
Regression (Rm)	3	3527.67	1175.89	217.19	0
Infill (I)	1	3282.29	3282.29	606.26	0
Layer Thickness (t)	1	38.64	38.64	7.14	0.011
Layer Thickness (t^2)	1	26.68	26.68	4.93	0.032
Error	41	221.97	5.41		
Lack-of-Fit	5	93.57	18.71	5.25	0.001
Pure Error	36	128.40	3.57		
Total	44	3749.64			

Figure 40 describes the impact of each term: A is the layer thickness and B is the infill; in this case, the infill has the most significant level of all the defined terms. The same result was reported in [33]. The significance of each term is expressed by its length in the chart. The vertical red line at 2.02 crosses all the bars representing the terms, which means that all terms impact on the determination of the regression model.

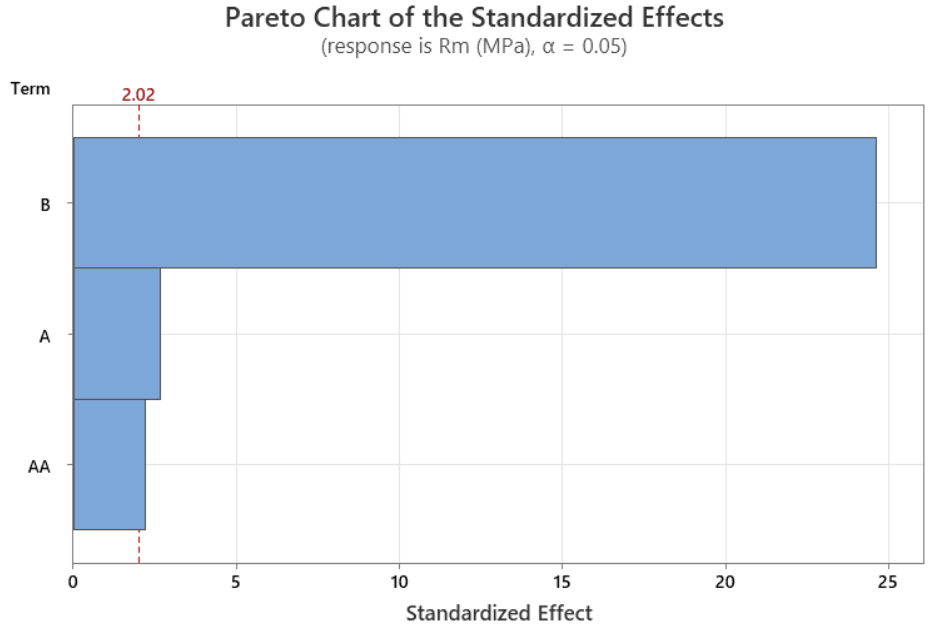

Figure 40. Pareto Chart of the regression model.

Figure 41 shows the graphs that describe the mathematical model: the first plot (a) checks whether the residuals are normally distributed. In this case, the assumption is verified because the residuals follow a straight line. The second plot (b) checks if the points of residuals are randomly distributed and on both sides of the 0-axis. Some patterns of residuals can be explained by the similar behavior of the specimens for the same parameters: infill and layer thickness. In the third plot (c), the chart describes the residual distribution. The last plot (d) verifies whether the residuals are independent from each other; in this case, the points of residuals are randomly distributed on both sides of the center line, indicating that the residuals are not correlated.

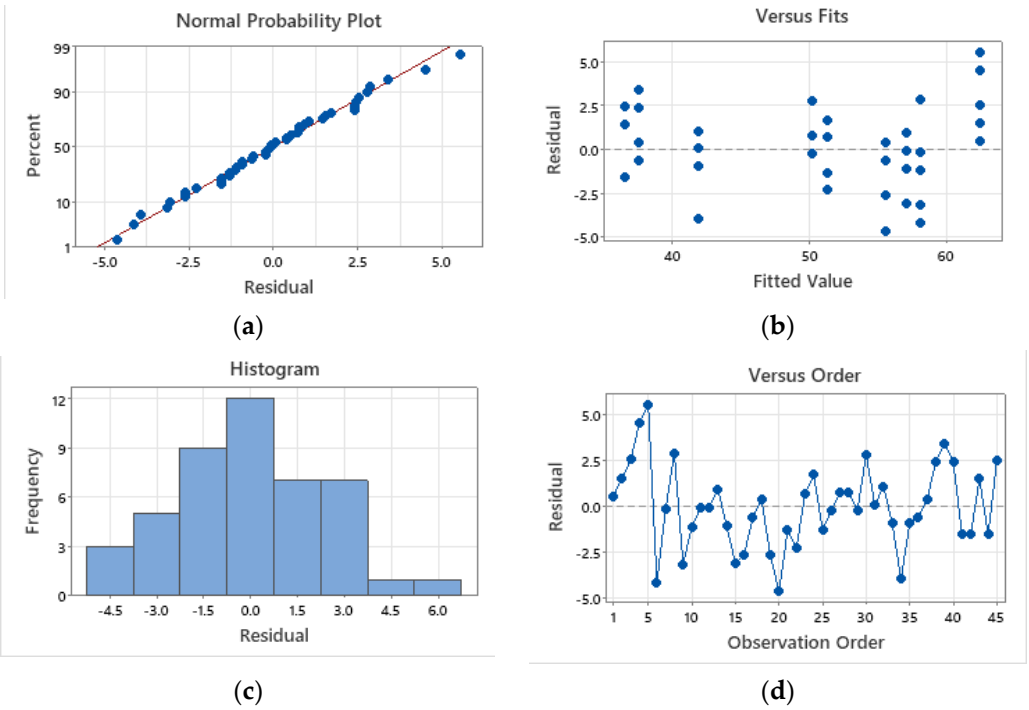

Figure 41. Residual Plots for Rm [MPa]: (**a**) Normal Probability Plot; (**b**) Versus Fits; (**c**) Histogram; (**d**) Versus Order.

4. Conclusions

The aim of this research is achieved by the performed tensile tests that took into account two of the most important manufacturing parameters, namely layer thickness and infill density. For each parameter three values were considered. For each parameter setpoint combination sets of 5 specimens were manufactured. The material was deposited along the longitudinal axis of the specimens.

The results are validated by a regression model obtained by an analysis of variance, classifying the studied parameters. Having obtained the values of the manufacturing parameters that yield the best results, further tensile tests are conducted to define the tensile values for specimens with material deposited along the transverse and thickness directions. In this manner the material can be described by all main directions, a novelty in the field, as in literature to date only few studies address composite filaments with PET matrices. After testing, specimens are visually checked under a microscope in order to identify manufacturing defects and rupture behavior.

The aspects discussed above yield the following conclusions:

- For the best results obtained for 100% infill and 0.15 mm layer thickness, further tensile tests were performed for specimens manufactured by material deposition in the transverse and thickness directions, because of the anisotropy of the material.

- The results in the longitudinal direction are: Rm = 65.4 MPa, Rp = 51.6 MPa, E = 9Gpa, ε = 1.93%.
- For the transverse direction the results are: Rm = 41–49 MPa, Rp = 9–45 MPa, E = 7 GPa, ε = 1–1.80%.
- For the thickness direction, the results are: Rm = 3 MPa, Rp = 1 MPa, E = 1 GPa and ε = 0.23%.
- If the material is deposited in a different direction than the direction of the load, the results are undesired and the geometrical stability is affected.
- Considering the conducted DOE, between layer thickness and infill density the most influential manufacturing parameter is infill.
- The reliability is influenced by the inconsistent results due to the defects that appear in all stages, from the raw material to the finite parts, these range from filament deviations to material voids and fiber conglomerates in both raw and finite materials.
- The most usual defect identified in each specimen are material voids. Due to material defects different failure modes occur during tensile loading, from layers debonding to material cracks or fibers dislocated from the matrix and brakeage.

The results of this research can be used in other studies concerned with the FEA process of complex products, as well as in manufacturing processes using this type of material and 3D printers. In further research the authors aim to describe the behavior at compression and bending of the same material, working with the most beneficial manufacturing parameter setpoints: layer thickness of 0.15 mm and infill density of 100%. In order to check the influence of carbon fibers on the mechanical properties and geometrical deviations, the same tests will be performed for specimens made from PET filaments.

Author Contributions: Conceptualization, M.-I.B. and G.O.; methodology, M.-I.B., S.-M.Z. and G.O.; software, M.-I.B.; validation, M.-I.B., C.O.M. and G.O.; formal analysis, M.-I.B.; investigation, M.-I.B., C.O.M., S.-M.Z., G.O. and M.C.; resources, M.A.P. and M.C.; writing—original draft preparation, M.-I.B.; writing—review and editing, M.-I.B. and G.O.; visualization, C.O.M., M.A.P. and M.C.; supervision, G.O. and S.-M.Z.; project administration, M.-I.B.; funding acquisition, G.O. All authors have read and agreed to the published version of the manuscript.

Funding: This research received no external funding.

Institutional Review Board Statement: Not applicable.

Data Availability Statement: Data are contained within the article.

Conflicts of Interest: The authors declare no conflict of interest.

Appendix A

The following figures present the tensile specimens before and after testing. The conclusions are discussed in Section 3.

(**a**) (**b**)

Figure A1. Longitudinal Tensile Specimens C_20_100: (**a**) Before testing; (**b**) After testing.

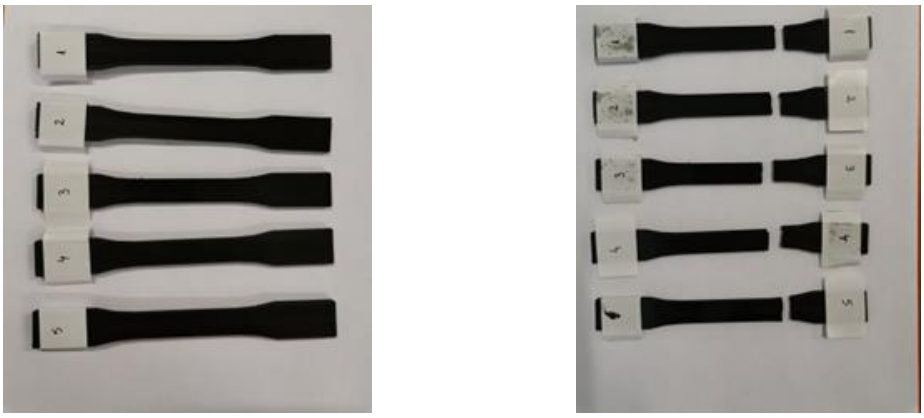

(**a**) (**b**)

Figure A2. Longitudinal Tensile Specimens C_25_100: (**a**) Before testing; (**b**) After testing.

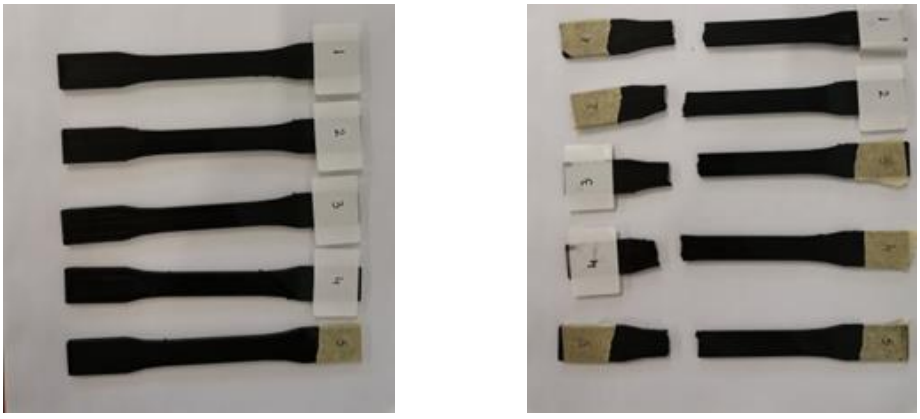

(**a**) (**b**)

Figure A3. Longitudinal Tensile Specimens C_15_75: (**a**) Before testing; (**b**) After testing.

(**a**) (**b**)

Figure A4. Longitudinal Tensile Specimens C_20_75: (**a**) Before testing; (**b**) After testing.

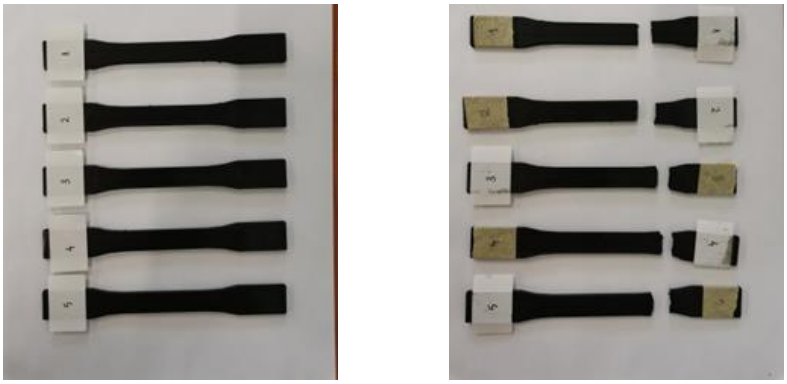

(**a**) (**b**)

Figure A5. Longitudinal Tensile Specimens C_25_75: (**a**) Before testing; (**b**) After testing.

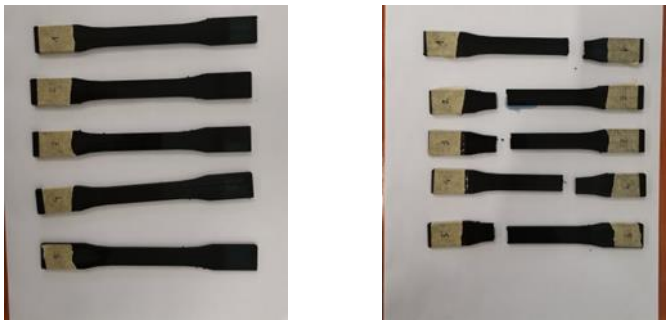

(**a**) (**b**)

Figure A6. Longitudinal Tensile Specimens C_15_25: (**a**) Before testing; (**b**) After testing.

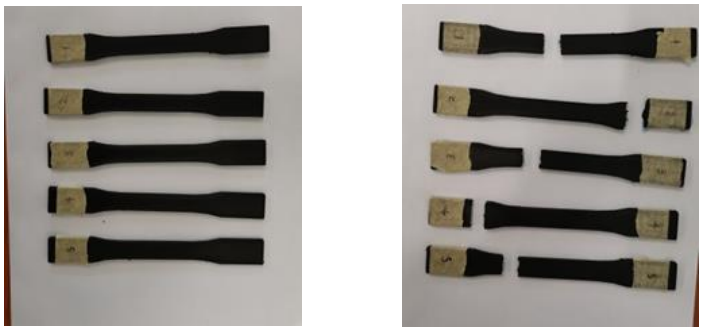

(**a**) (**b**)

Figure A7. Longitudinal Tensile Specimens C_20_25: (**a**) Before testing; (**b**) After testing.

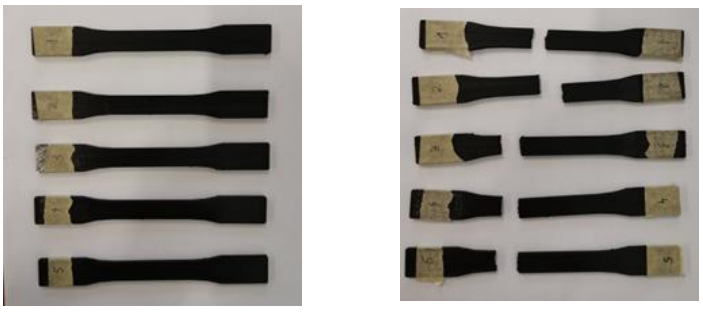

(**a**) (**b**)

Figure A8. Longitudinal Tensile Specimens C_25_25: (**a**) Before testing; (**b**) After testing.

Appendix B

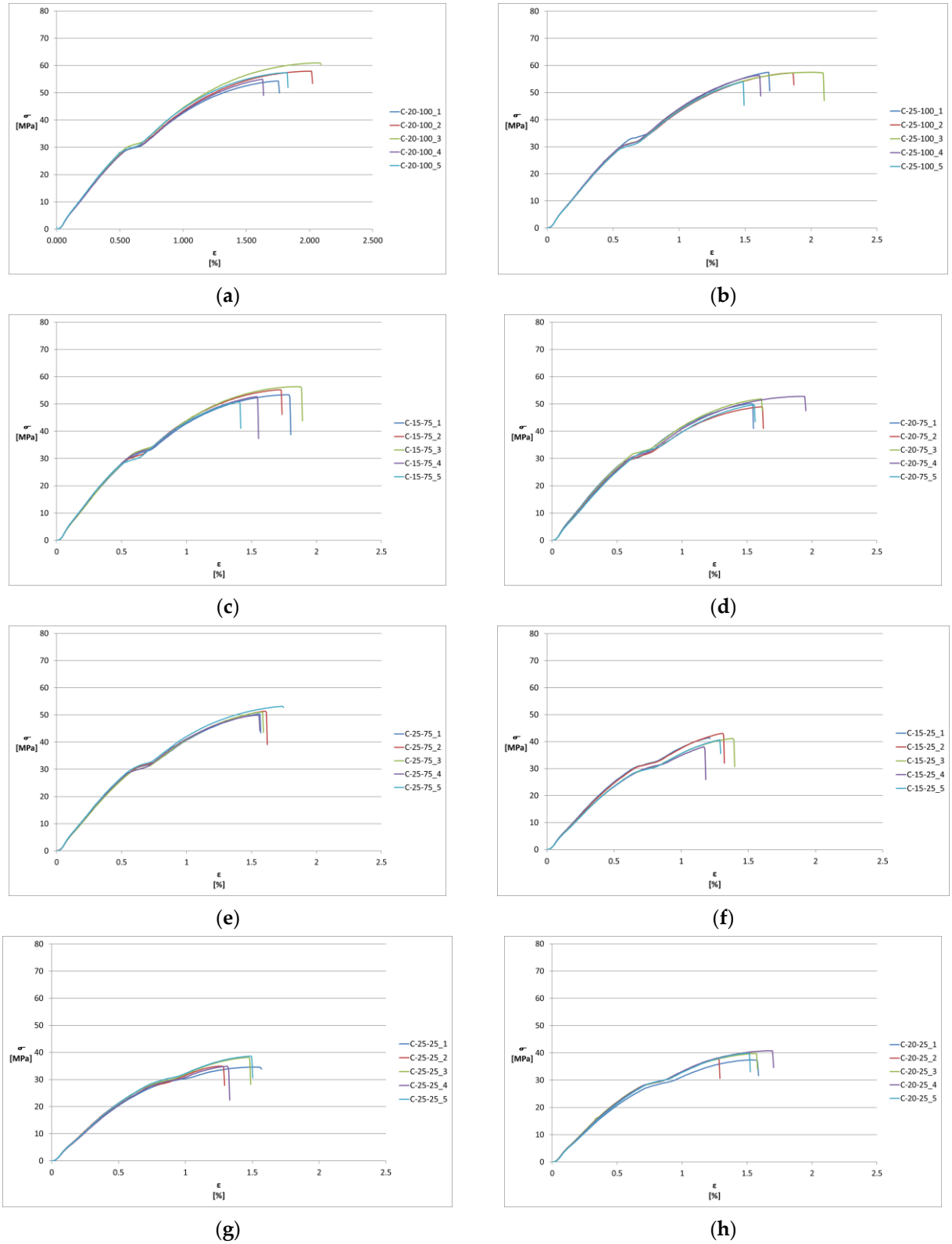

Figure A9. Longitudinal Tensile Specimens results–Stress-Strain curves: (**a**) Stress-Strain curves for C_20_100; (**b**) Stress-Strain curves for C_25_100; (**c**) Stress-Strain curves for C_15_75; (**d**) Stress-Strain curves for C_20_75; (**e**) Stress-Strain curves for C_25_75; (**f**) Stress-Strain curves for C_15_25; (**g**) Stress-Strain curves for C_20_25; (**h**) Stress-Strain curves for C_25_25.

Table A1. Longitudinal Tensile Specimens Result–C_20_100.

Specimen	Fm (kN)	Rm (MPa)	Fp (kN)	Rp(kN)	E (GPa)	ε (%)
C_20_100_1	2.402	54	1.573	36	9	1.77
C_20_100_2	2.562	58	1.702	38	9	2.03
C_20_100_3	2.695	61	1.821	41	9	2.11
C_20_100_4	2.429	55	1.621	37	9	1.64
C_20_100_5	2.538	57	1.737	39	9	1.84
Mean	2.53	57.00	1.69	38.20	9	1.88

Table A2. Longitudinal Tensile Specimens Result—C_25_100.

Specimen	Fm (kN)	Rm (MPa)	Fp (kN)	Rp(kN)	E (GPa)	ε (%)
C_25_100_1	2.483	57	1.629	38	9	1.69
C_25_100_2	2.474	57	1.614	37	9	1.88
C_25_100_3	2.484	58	1.622	38	9	2.11
C_25_100_4	2.431	56	1.632	38	9	1.62
C_25_100_5	2.328	54	1.589	37	9	1.50
Mean	2.44	56.40	1.62	37.20	9	1.76

Table A3. Longitudinal Tensile Specimens Result—C_15_75.

Specimen	Fm (kN)	Rm (MPa)	Fp (kN)	Rp(kN)	E (GPa)	ε (%)
C_15_75_1	2.238	53	1.811	43	8	1.8
C_15_75_2	2.314	55	1.534	37	10	1.74
C_15_75_3	2.363	56	1.555	37	9	1.90
C_15_75_4	2.209	53	1.45	35	10	1.55
C_15_75_5	2.126	51	1.469	35	10	1.42
Mean	2.25	53.60	1.56	37.40	9.40	1.68

Table A4. Longitudinal Tensile Specimens Result—C_20_75.

Specimen	Fm (kN)	Rm (MPa)	Fp (kN)	Rp(kN)	E (GPa)	ε (%)
C_20_75_1	2.133	50	1.435	34	9	1.56
C_20_75_2	2.084	49	1.407	33	9	1.63
C_20_75_3	2.207	52	1.468	34	9	1.62
C_20_75_4	2.248	53	1.471	35	9	1.96
C_20_75_5	2.115	50	1.46	34	9	1.57
Mean	2.16	50.80	1.45	34.00	9	1.67

Table A5. Longitudinal Tensile Specimens Result—C_25_75.

Specimen	Fm (kN)	Rm (MPa)	Fp (kN)	Rp(kN)	E (GPa)	ε (%)
C_25_75_1	2.139	50	1.435	34	9	1.58
C_25_75_2	2.180	51	1.471	35	9	1.620
C_25_75_3	2.166	51	1.448	34	9	1.60
C_25_75_4	2.117	50	1.429	34	9	1.57
C_25_75_5	2.255	53	1.493	35	9	1.75
Mean	2.17	51.00	1.46	34.40	9	1.62

Table A6. Longitudinal Tensile Specimens Result—C_15_25.

Specimen	Fm (kN)	Rm (MPa)	Fp (kN)	Rp(kN)	E (GPa)	ε (%)
C_15_25_1	1.686	42	1.305	32	9	1.21
C_15_25_2	1.748	43	1.303	32	9	1.32
C_15_25_3	1.670	41	1.229	30	8	1.40
C_15_25_4	1.545	38	1.255	31	8	1.18
C_15_25_5	1.649	41	1.224	30	8	1.30
Mean	1.66	41	1.26	31	8.40	1.28

Table A7. Longitudinal Tensile Specimens Result—C_20_25.

Specimen	Fm (kN)	Rm (MPa)	Fp (kN)	Rp(kN)	E (GPa)	ε (%)
C_20_25_1	1.616	37	1.235	29	7	1.60
C_20_25_2	1.631	38	1.280	30	8	1.30
C_20_25_3	1.719	40	1.254	29	8	1.59
C_20_25_4	1.762	41	1.269	29	8	1.71
C_20_25_5	1.723	40	1.291	30	7	1.53
Mean	1.69	39.20	1.27	29.40	7.60	1.55

Table A8. Longitudinal Tensile Specimens Result—C_25_25.

Specimen	Fm (kN)	Rm (MPa)	Fp (kN)	Rp(kN)	E (GPa)	ε (%)
C_25_25_1	1.472	35	1.224	29	7	1.58
C_25_25_2	1.487	35	1.196	28	7	1.29
C_25_25_3	1.626	38	1.253	29	7	1.49
C_25_25_4	1.484	35	1.237	29	7	1.33
C_25_25_5	1.645	39	1.282	30	7	1.50
Mean	1.54	36.40	1.24	29	7	1.44

Table A9. Longitudinal Tensile Specimens Result—C_20_100—Deviations from the mean value.

Specimen	Fm [%]	Rm [%]	Fp [%]	Rp [%]	E [%]	ε [%]
C_20_100_1	−4.88	−5.26	−6.97	−5.76	0.00	−5.75
C_20_100_2	1.46	1.75	0.66	−0.52	0.00	8.09
C_20_100_3	6.72	7.02	7.70	7.33	0.00	12.35
C_20_100_4	−3.81	−3.51	−4.13	−3.14	0.00	−12.67
C_20_100_5	0.51	0.00	2.73	2.09	0.00	−2.02

Table A10. Longitudinal Tensile Specimens Result—C_25_100—Deviations from the mean value.

Specimen	Fm [%]	Rm [%]	Fp [%]	Rp [%]	E [%]	ε [%]
C_25_100_1	1.76	1.06	0.73	1.06	0.00	−3.98
C_25_100_2	1.39	1.06	−0.20	−1.60	0.00	6.82
C_25_100_3	1.80	2.84	0.30	1.06	0.00	19.89
C_25_100_4	−0.37	−0.71	0.92	1.06	0.00	−7.95
C_25_100_5	−4.59	−4.26	−1.74	−1.60	0.00	−14.77

Table A11. Longitudinal Tensile Specimens Result—C_15_75—Deviations from the mean value.

Specimen	Fm [%]	Rm [%]	Fp [%]	Rp [%]	E [%]	ε [%]
C_15_75_1	−0.53	−1.12	15.81	14.97	−14.89	7.02
C_15_75_2	2.84	2.61	−1.91	−1.07	6.38	3.45
C_15_75_3	5.02	4.48	−0.56	−1.07	−4.26	12.96
C_15_75_4	−1.82	−1.12	−7.28	−6.42	6.38	−7.85
C_15_75_5	−5.51	−4.85	−6.06	−6.42	6.38	−15.58

Table A12. Longitudinal Tensile Specimens Result—C_20_75—Deviations from the mean value.

Specimen	Fm [%]	Rm [%]	Fp [%]	Rp [%]	E [%]	ε [%]
C_20_75_1	−1.13	−1.57	−0.91	0.00	0.00	−6.47
C_20_75_2	−3.40	−3.54	−2.84	−2.94	0.00	−2.28
C_20_75_3	2.30	2.36	1.37	0.00	0.00	−2.88
C_20_75_4	4.20	4.33	1.57	2.94	0.00	17.51
C_20_75_5	−1.97	−1.57	0.81	0.00	0.00	−5.88

Table A13. Longitudinal Tensile Specimens Result—C_25_75—Deviations from the mean value.

Specimen	Fm [%]	Rm [%]	Fp [%]	Rp [%]	E [%]	ε [%]
C_25_75_1	−1.49	−1.96	−1.39	−1.16	0.00	−2.71
C_25_75_2	0.40	0.00	1.09	1.74	0.00	−0.25
C_25_75_3	−0.25	0.00	−0.49	−1.16	0.00	−1.48
C_25_75_4	−2.51	−1.96	−1.80	−1.16	0.00	−3.33
C_25_75_5	3.85	3.92	2.60	1.74	0.00	7.76

Table A14. Longitudinal Tensile Specimens Result—C_15_25—Deviations from the mean value.

Specimen	Fm [%]	Rm [%]	Fp [%]	Rp [%]	E [%]	ε [%]
C_15_25_1	1.59	2.44	3.31	3.23	7.14	−5.62
C_15_25_2	5.33	4.88	3.15	3.23	7.14	2.96
C_15_25_3	0.63	0.00	−2.71	−3.23	−4.76	9.20
C_15_25_4	−6.91	−7.32	−0.65	0.00	−4.76	−7.96
C_15_25_5	−0.64	0.00	−3.10	−3.23	−4.76	1.40

Table A15. Longitudinal Tensile Specimens Result—C_20_25—Deviations from the mean value.

Specimen	Fm [%]	Rm [%]	Fp [%]	Rp [%]	E [%]	ε [%]
C_20_25_1	−4.39	−5.61	−2.43	−1.36	−7.89	3.49
C_20_25_2	−3.50	−3.06	1.12	2.04	5.26	−15.91
C_20_25_3	1.70	2.04	−0.93	−1.36	5.26	2.85
C_20_25_4	4.25	4.59	0.25	−1.36	5.26	10.61
C_20_25_5	1.94	2.04	1.99	2.04	−7.89	−1.03

Table A16. Longitudinal Tensile Specimens Result—C_25_25—Deviations from the mean value.

Specimen	Fm [%]	Rm [%]	Fp [%]	Rp [%]	E [%]	ε [%]
C_25_25_1	−4.59	−3.85	−1.16	0.00	0.00	9.87
C_25_25_2	−3.62	−3.85	−3.42	−3.45	0.00	−10.29
C_25_25_3	5.39	4.40	1.18	0.00	0.00	3.62
C_25_25_4	−3.81	−3.85	−0.11	0.00	0.00	−7.51
C_25_25_5	6.62	7.14	3.52	3.45	0.00	4.31

Appendix C

Table A17. Design of Experiments—Independent variable values.

Run Order	Infill [%]	Layer Thickness [mm]
1	75	0.25
2	100	0.15
3	100	0.15
4	75	0.15
5	100	0.2

Table A17. *Cont.*

Run Order	Infill [%]	Layer Thickness [mm]
6	100	0.2
7	75	0.15
8	75	0.2
9	25	0.25
10	100	0.2
11	25	0.15
12	75	0.2
13	25	0.15
14	25	0.2
15	75	0.15
16	75	0.2
17	100	0.25
18	100	0.25
19	25	0.15
20	100	0.25
21	75	0.25
22	100	0.15
23	75	0.25
24	25	0.25
25	25	0.25
26	25	0.25
27	75	0.2
28	100	0.25
29	25	0.2
30	25	0.15
31	25	0.2
32	75	0.2
33	100	0.25
34	100	0.15
35	100	0.15
36	75	0.25
37	25	0.15
38	75	0.15
39	100	0.2
40	25	0.25
41	25	0.2
42	100	0.2
43	75	0.25
44	75	0.15
45	75	0.25

References

1. García, E.; Núñez, P.; Caminero, M.; Chacón, J.; Kamarthi, S. Effects of carbon fibre reinforcement on the geometric properties of PETG-based filament using FFF additive manufacturing. *Compos. Part B Eng.* **2022**, *235*, 109766. [CrossRef]
2. Spoerk, M.; Savandaiah, C.; Arbeiter, F.; Traxler, G.; Cardon, L.; Holzer, C.; Sapkota, J. Anisotropic properties of oriented short carbon fibre filled polypropylene parts fabricated by extrusion-based additive manufacturing. *Compos. A Appl. Sci. Manuf.* **2018**, *113*, 95–104. [CrossRef]
3. Wang, P.; Zou, B.; Ding, S.; Hunag, C.; Shi, Z.; Ma, Y.; Yao, P. Preparation of short CF/GF reinforced PEEK composite filaments and their comprehensive properties evaluation for FDM-3D printing. *Compos. Part B* **2020**, *198*, 108175. [CrossRef]
4. Blaj, M.; Oancea, G. Fused deposition modelling process: A literature review. *IOP Conf. Ser. Mater. Sci. Eng.* **2021**, *1009*, 012006. [CrossRef]
5. Bembenek, M.; Kowalski, Ł.; Kosoń-Schab, A. Research on the Influence of Processing Parameters on the Specific Tensile Strength of FDM Additive Manufactured PET-G and PLA Materials. *Polymers* **2022**, *14*, 2446. [CrossRef]
6. Soleyman, E.; Rahmatabadi, D.; Soltan Mohammadi, K.; Aberoumand, M.; Ghasemi, I.; Abrinia, K.; Baniassadi, M.; Wang, K.; Baghani, M. Shape memory performance of PETG 4D printed parts under compression in cold, warm, and hot programming. *Smart Mater. Struct.* **2022**, *31*, 85002. [CrossRef]

7. Muhamedagic, K.; Berus, L.; Potočnik, D.; Cekic, A.; Begic-Hajdarevic, D.; Cohodar Husic, M.; Ficko, M. Effect of Process Parameters on Tensile Strength of FDM Printed Carbon Fiber Reinforced Polyamide Parts. *Appl. Sci.* **2022**, *12*, 6028. [CrossRef]
8. Krajangsawasdi, N.; Blok, L.G.; Hamerton, I.; Longana, M.L.; Woods, B.K.S.; Ivanov, D.S. Fused deposition modelling of fibre reinforced polymer composites: A parametric review. *J. Compos. Sci.* **2021**, *5*, 29. [CrossRef]
9. R, M.K.H.; Benal, M.G.M.; G.S., P.K.; Tambrallimath, V.; H.R., G.; Khan, T.M.Y.; Rajhi, A.A.; Baig, M.A.A. Influence of Short Glass Fibre Reinforcement on Mechanical Properties of 3D Printed ABS-Based Polymer Composites. *Polymers* **2022**, *14*, 1182.
10. Rahimizadeh, A.; Kalman, J.; Fayazbakhsh, K.; Lessard, L. Recycling of fiberglass wind turbine into reinforced filaments for use in Additive Manufacturing. *Compos. Part B Eng.* **2019**, *175*, 107101. [CrossRef]
11. Kalman, J.; Fayazbakhsh, K.; Rahimizadeh, A.; Lessard, L. Mechanical and thermal study of 3D printing composite filaments from wind turbine waste. *Polym. Compos.* **2021**, *42*, 2305–2316.
12. Vedrtnam, A.; Ghabezi, P.; Gunwant, D.; Jiang, Y.; Sam-Daliri, O.; Harrison, N.; Goggins, J.; Finnegan, W. Mechanical performance of 3D-printed continuous fibre Onyx composites for drone applications: An experimental and numerical analysis. *Compos. Part C* **2023**, *12*, 100418. [CrossRef]
13. Hou, Y.; Panesar, A. Effect of Manufacture-Induced Interfaces on the Tensile Properties of 3D Printed Polyamide and Short Carbon Fibre-Reinforced Polyamide Composites. *Polymers* **2023**, *15*, 773. [CrossRef]
14. Mollah, M.T.; Comminal, R.; Serdeczny, M.P.; Šeta, B.; Spangenberg, J. Computational analysis of yield stress buildup and stability of deposited layers in material extrusion additive manufacturing. *Addit. Manuf.* **2023**, *71*, 4–11.
15. Rahmatabadi, D.; Soltanmohammadi, K.; Aberoumand, M.; Soleyman, E.; Ghasemi, I.; Baniassadi, M.; Abrinia, K.; Bodaghi, M.; Baghani, M. Development of Pure Poly Vinyl Chloride (PVC) with Excellent 3D Printability and Macro- and Micro-Structural Properties. *Macromol. Mater. Eng.* **2022**, *308*, 2200568. [CrossRef]
16. Blaj, M.I.; Zaharia, S.M.; Pop, M.A.; Oancea, G. Tensile Properties and Manufacturing Defectives of Short Carbon Fiber Specimens Made with the FDM Process. *Mater. Plast.* **2022**, *59*, 33–43. [CrossRef]
17. Jiang, D.; Smith, D. Anisotropic mechanical properties of oriented carbon fiber filled polymer composites produced with fused filament fabrication. *Addit. Manuf.* **2017**, *18*, 84–94. [CrossRef]
18. Ritter, T.; McNiffe, E.; Higgins, T.; Sam-Daliri, O.; Flanagan, T.; Walls, M.; Ghabezi, P.; Finnegan, W.; Mitchel, S.; Harrison, N.M. Design and Modification of a Material Extrusion 3D Printer to Manufacture Functional Gradient PEEK Components. *Polymers* **2023**, *15*, 3825. [CrossRef]
19. Cao, M.; Cui, T.; Yue, Y.; Li, C.; Guo, X.; Jia, X.; Wang, B. Investigation of Carbon Fiber on the Tensile Property of FDM-Produced PLA Specimen. *Polymers* **2022**, *14*, 5230. [CrossRef]
20. Mishra, D.; Das, A.K. Linear model analysis of fused deposition modeling process parameters for obtaining the maximum tensile strength in acrylonitrile butadiene styrene (ABS) and carbon fiber polylactic acid (PLA) materials. *Multidiscip. Model. Mater. Struct.* **2021**, *17*, 915–930. [CrossRef]
21. Patterson, A.E.; Hasanov, S.; Vajipeyajula, B. Influence of Matrix Material on Impact Properties of Chopped Carbon Fiber-Thermoplastic Composites made using FDM/FFF. In Proceedings of the 2022 International Additive Manufacturing Conference, Lisbon, Portugal, 19–20 October 2022; pp. 1–8. [CrossRef]
22. Omar, N.W.Y.; Shuaib, N.A.; Hadi, M.H.J.A.; Azmi, A.I.; Misbah, M.N. Mechanical and Physical Properties of Recycled-Carbon-Fiber-Reinforced Polylactide Fused Deposition Modelling Filament. *Materials* **2022**, *15*, 190. [CrossRef]
23. Saschit, T.S.; Mukul Ramnirajan Saini, D. Vinaykumar, Effect of Printing Parameters on Tensile Strength of 3D Printed PLA + Carbon Fiber Samples—A Taguchi Approach. In *Recent Developments in Mechanical Design*; Springer: Singapore, 2022; pp. 1–3. [CrossRef]
24. Abeykoon, C.; Abeykoon, C.; Fernando, A. Optimization of fused deposition modeling parameters for improved PLA and ABS 3D printed structures. *Int. J. Light. Mater. Manuf.* **2020**, *3*, 284–297. [CrossRef]
25. Unterweger, C.; Mayrhofer, T.; Piana, F.; Duchoslav, J.; Stifter, D.; Poitzsch, C.; Fürst, C. Impact of fiber length and fiber content on the mechanical properties and electrical conductivity of short carbon fiber reinforced polypropylene composites. *Compos. Sci. Technol.* **2020**, *188*, 107998. [CrossRef]
26. Katalagarianakis, A.; Van de Voorde, B.; Pien, N.; Polyzos, E.; Duretek, I.; Holzer, C.; Cardon, L.; Bernaerts, K.V.; Van Hemelrijck, D.; Van Vlierberghe, S.; et al. The Effect of Carbon Fiber Content on Physico-Mechanical Properties of Recycled PolyEthylene Terephthalate) Composites Additively Manufactured with Fused Filament Fabrication. *Addit. Manuf.* **2022**, *60*, 103246.
27. Ultrafuse Filaments. Available online: https://forward-am.com/material-portfolio/ultrafuse-filaments-for-fused-filaments-fabrication-fff/reinforced-filaments/ultrafuse-pet-cf15/ (accessed on 10 April 2023).
28. ASTM International. Standard Test Method for Tensile Properties of Plastics (Metric). Available online: https://www.astm.org/d0638-14.html (accessed on 25 January 2024).
29. BCN3D Technologies. Available online: https://www.bcn3d.com/bcn3d-epsilon/?model=w50 (accessed on 17 April 2023).
30. Tuttle, M.E. *Structural Analysis of Polymeric Composite Materials*, 2nd ed.; CRC Press: Boca Raton, FL, USA, 2012.
31. Mohan, S.R.; Simhambhatla, S. Fabrication of gradient density componenets through extrusion—Based additive manufacturing. In *Advances in Additive Manufacturing and Joining Proceedings of AIMTDR 2018*; Springer: Singapore, 2019; pp. 181–182.

32. Belei, C.; Joeressen, J.; Amancio-Filho, S.T. Fused-Filament Fabrication of Short Carbon Fiber-Reinforced Polyamide: Parameter Optimization for Improved Performance under Uniaxial Tensile Loading. *Polymers* **2022**, *14*, 1292. [CrossRef]
33. Algarni, M.; Ghazali, S. Comparative study of the sensitivity of PLA, ABS, PEEK, and PETG's mechanical properties to FDM printing process parameters. *Crystals* **2021**, *11*, 995. [CrossRef]